SSRG International Journal of Civil Engineering
ISSN: 2348-8352/ https://doi.org/10.14445/23488352/IJCE-V13I7P119

Volume 13 Issue 7, 297-322, July 2026

Original Article

Spatio-Temporal Reservoir Water Quality Assessment Using PSO-Adam Optimized Vision Transformers

Sachchidanand Bhagat[1], L. B. Roy[2]

[1,2]*Department of Civil Engineering, National Institute of Technology Patna (NIT Patna), Patna, Bihar, India.*

[1]*Corresponding Author : sachchidanandb.phd20.ce@nitp.ac.in*

Received: 27 December 2025 Revised: 01 June 2026 Accepted: 04 July 2026 Published: 29 July 2026

Abstract *- Continuous Water Quality (WQ) monitoring and measurement in dam reservoirs at different locations in the same dam water regions are the major problem. Spatial heterogeneity led to variations in WQ metrics such as pH, DO, TDS in the dam reservoir based on different depths due to sedimentation and nutrient cycling. Manual sampling methods is not suitable for continues WQ parameter measuring in different locations of dam water regions. To solve the above problem, Landsat image of dam water regions is processed with the Transverse Dyadic Wavelet Transform (TDyWT) and the Adam Optimized Vision Transformer (AdamViT) algorithms and obtained the statistical features of water regions for the temporal and spatial regions. Nagi Dam (NGD) and Nakti Dam (NKD) reservoirs in Bihar, India is the study area for the proposed study. The statistical values of water regions measured are the mean, entropy, PSNR, band values. The obtain statistical water feature values are correlated with laboratory-based sample water measured four WQ metrics. AdamViT- Bayesian Optimised-(BO)- (Support Vector Regression) SVR predicts the above four Key WQ metrics. AdamViT- BO-SVR provide the R2 value 0.97, RMSE is 0.15, and MAPE is 3.4% compared to the ground truth.*

Keywords *- Water Quality metrics measurement, Wavelet Transform, Vision Transformer, Support Vector Regression.*

1. Introduction

Dam waters are used for agriculture. For organic cultivation and to increase the productivity of the crops, Water Quality (WQ) plays a vital role. Continuous WQ in the dam reservoirs need to be performed for WQ management. WQ in dam reservoirs is contaminated due to sprawl expansions, expanding of industries and climate change [1]. Heavy metals, pesticides, sedimentation drifts, and pathogens contaminate the water in dams [2]. Dam WQ is performed manual sample water collection and testing of sample water done in the laboratory [3]. In dam water, turbidity, TSS, pH, conductivity, temperature, chlorophyll concentration, DO, nutrients, namely the nitrogen and phosphorus, organic matter, heavy metals [4, 5] need to be measured on regularly for WQ management. WQ management in dams will protect groundwater contamination. metal ions in dam water, such as Lead (Pb), Zinc (Zn), and Manganese (Mn), are needing large sample collection in different locations of dam water area [6, 7]. Sedimentation drift elevates contaminants level in dam water. Maximum metals in dam water are Pb: 0.1-0.5 mg/L, Zn: 2-5 mg/L, and Mn: 0.2-1.0 mg/L. Maintaining the metal limits leads to organic cultivation and improves the ground WQ. Low concentrations of metal in water damage the digestive systems of animals and humans [8]. Plants watered with heavy metals lead to low yield and nutrients food grains/ fruits. Consumption of agricultural products grown in metal water damages the neurons and leads to gastrointestinal problems and fertility problems [9, 10].

Traditional methods of WQ metric measurement are performed by the sample collection and laboratory-based water samples measurement values, which are time-consuming and never repeated for the same locations and different locations of water regions in dams. The sample-based measurement does not provide an accurate measurement due to the geographical and temporal variations [11]. Furthermore, interdisciplinary collaboration can enhance the accuracy and efficiency of WQ management in dams [12]. Table 1 shows the Key WQ metrics To Be Monitored.

Remote sensing methods used for the chlorophyll a measure through correlations with statistical parameters [14]. WQ is reduced due to stratification, sedimentation, and nutrient cycling [15]. Stratification prevents mixing of water layers and leads to low oxygen in the water layers. Sedimentation changes the chemical compositions in water [16]. The spatial and temporal WQ monitoring using a wireless floating sensor is not accurate due to the frequent movement of the sensor in the water region. Microclimate condition increases the pollutants in water [17, 18]. WQ safeguards human health [19]. Table 2 shows the acceptable level of metal in dams/reservoirs.

1.1. Research Gap

WQ monitoring in dams/ water reservoirs has a significant gap due to manual sampling. Sensor-based systems are insufficient for comprehensive data collection from the dam waters in different depth and locations. existing methods depend on limited datasets and never consider the physical, chemical, and biological factors, and water dynamics. Need an accurate method for WQ monitoring in dams/ water reservoirs. Addressing the above gaps needs an efficient WQ management and monitoring method in dam reservoirs. Table 3 shows a description of the research gap.

Table 1. Primary WQ parameters for monitoring

Key WQ metrics [13]	Parameter to be monitored in the water
Physical	Water temperature, transparency, salinity, turbidity, total suspended matter, colored dissolved organic matter, odor, and electrical conductivity.
Chemical	pH, Dissolved Oxygen (DO), chemical oxygen demand, biochemical oxygen demand, total nitrogen, total phosphorus, heavy metals, and non-metallic toxins.
Biological	Chlorophyll-a, total bacteria count, and total coliforms.

Table 2. Heavy metals monitored in indian dam reservoirs

Metal	Ambient target limit in lake/dam (mg/L) *	Basis/reference use
Arsenic (As)	0.01	BIS IS 10500:2012 acceptable limit for drinking water; used as benchmark for Class A/C sources.
Lead (Pb)	0.01	BIS IS 10500 drinking-water limits, applied to lake/dam water used for supply.
Cadmium (Cd)	0.003	BIS IS 10500 drinking-water limits; no relaxation.
Chromium (total, as Cr)	0.05	BIS IS 10500 drinking-water limits.
Mercury (Hg)	0.001	BIS IS 10500 drinking-water limits.
Nickel (Ni)	0.02	Trace-metal benchmark in national surface-water assessments.
Selenium	0.01	Drinking-water guideline used for Class A/C sources.
Iron	0.3	Aesthetic/operational limit from BIS IS 10500.
Manganese	0.1	BIS IS 10500 guidelines for drinking water.
Copper	0.05 (desirable), up to 1.0 (max)	BIS IS 10500 drinking-water limits.
Zinc (Zn)	5.0 (desirable), up to 15.0 (max)	Mainly aesthetic; BIS IS 10500.

1.2. Problems in Continuous Water Monitoring in Dam Waters

Landsat data is of low spatial resolution, makes hard for detection of small pollution level in water bodies. Temporal resolution changes the WQ. Weather conditions such as clouds and haze obstruct satellite images and lead to inaccurate WQ monitoring. Vegetation in reservoir areas complicates the WQ measurement.

The above problem needs to be explored in Nagi Dam (NGD) and Nakti Dam (NKD) and, where water moss is present. To address the above problem proposed method integrates both spatial and temporal pixels and applied proposed Transverse Dyadic Wavelet Transform (TDyWT) with an optimized Vision Transformer algorithms monitored the WQ metrics. Table 4 shows problem in the WQ metric measurement and description. Table 5 shows limitations with solution through the proposed method.

Table 3. Research gaps in reservoir WQ monitoring

Existing method	Research Gap	Proposed Solution
Manual Sampling	Limited spatial and temporal coverage	Multi-temporal Landsat monitoring
Sensor Monitoring	Limited depth and spatial coverage	Satellite-based reservoir assessment
Remote Sensing	Limited feature extraction capability	TDyWT image enhancement
ML Models	Small datasets and low generalization	BO-SVR integration framework
Water-Vegetation Separation	Poor discrimination of water and moss	AdamViT + DTGC segmentation
Spatio-Temporal Analysis	Reservoir dynamics insufficiently addressed	Spatial-temporal feature integration
Validation	Limited laboratory verification	Field-data-based validation
Reservoir Management	Lack of real-time monitoring support	Automated prediction framework

Table 4. Challenges in WQ measurement

Problems	Description
Low Resolution	Satellite images hinder small pollution detection
Temporal Changes	Resolution variations affect WQ assessment.
Weather Interference	Clouds/haze obstruct satellite imagery accuracy.
Vegetation Issues	Water moss complicates measurements in reservoirs.
Study Focus	Explored specifically in NGD and NKD
Proposed Solution	TDyWT + optimized ViT integrates spatial/temporal pixels.

Table 5. Limitations and proposed method solutions

Limitations in dam WQ measurement	Proposed method solution to the limitations
Low spatial resolution	TDyWT enhances spatial detail to detect small polluted regions.
Temporal variation in WQ	Spatio-temporal pixel integration stabilizes quality monitoring.
Clouds and haze	Optimized ViTs suppress atmospheric noise and clarify features.
Vegetation (water moss) interference	DTGC separates water and moss for clean feature extraction.
Weak link to lab parameters	BOSVR maps image features to measured WQ and lead.

1.3. Contributions

The major contributions are:

To collect comprehensive Key WQ metrics at multiple locations in the NGD and NKD reservoirs, alongside lead content analysis from water moss leaf samples to assess contamination impacts.

To enhance Landsat imagery spatial resolution via the proposed TDyWT perspective projection, and refine water/moss pixels using the proposed Adam Optimized Vision Transformer (AdamViT) for accurate reservoir monitoring

To segment water versus moss regions with a dual-threshold graph cut method, extract statistical pixel features, and correlate with laboratory data through the proposed AdamViT-SVR method, and validate predictions with ground truth verification. Table 6 shows the Proposed Method Components

Table 6. Proposed method components

Proposed Method	Contribution	Novelty
Data Collection	Lab parameters + moss lead content	Combines WQ and bioindicator data
TDyWT Projection	Enhances Landsat images	Improves water-moss separation
Pixel Enhancement	PSOViT/AdamViT	Optimized ViT for low-resolution imagery
Region Extraction	DTGC segmentation	More accurate water-moss delineation
Prediction Model	BO-SVR	Fuses image and laboratory data
Validation	Benchmark comparison	Validated with field measurements

1.3.1. Novelty

- Integrated remote sensing bioindicator framework for heavy metal assessment
- TDyWT for perspective-aware spatial enhancement
- Dual-Threshold Graph Cut (DTGC) for fine-grained water moss segmentation
- Bayesian-optimized SVR for fusing image features with laboratory measurements
- Comprehensive comparative validation on real dam reservoirs

2. Literature Survey

Recent research focused on different methods for WQ monitoring is tabulated in Table 7. These studies highlight the effectiveness of different methods for accurate and timely measurement of WQ. Table 8 shows the proposed method with traditional method comparison.

Previous research, such as regression models, random forests, support vector machines, XGBoost, hyperspectral imaging, and cloud-based monitoring systems used for assessing WQ parameters [36-38]. Limitations of the above are spatial coverage, temporal variability, dataset size, vegetation interference, and integration of laboratory measurements with remote sensing data. Table 8 highlights the hybridization of image processing, machine learning, and field observations to improve the accuracy of reservoir WQ monitoring.

Existing WQ monitoring methods have limitations, such as spatial and temporal coverage. The above limitations in reservoir WQ assessment are still continued. To address the above problem, this study integrates AdamViT-BO-SVR with TDyWT-based image enhancement, DTGC-based water-moss segmentation, and Bayesian-optimized SVR prediction uses Landsat image and laboratory values. The proposed method was applied in the NGD and NKD reservoirs.

3. Methods

The proposed methodology integrates Landsat image pixels statistical values, water sample laboratory values. The Landsat image is processed with the proposed optimized Vision Transformer (ViT) method and a regression method for WQ parameter prediction. Continuous monitoring of WQ in NGD and NKD reservoirs is proposed as shown in Figure 1. The proposed method comprises of (i) Landsat image collection based on temporal and spatial water regions of NGD and NKD reservoirs with moss in the image. (ii) Feature extraction detects water moss. (iii) Optimized transform model used for the prediction of WQ. (iv) Predictions Key WQ metrics are performed using AdamViT + BOSVR. The proposed method monitors WQ parameters using water moss. Multi-temporal Landsat images are enhanced using TDyWT, applied with PSOViT/AdamViT and DTGC for water moss segmentation, and combined with laboratory measurements in a BO-SVR model to accurately predict WQ parameters such as pH, DO, TDS, and conductivity.

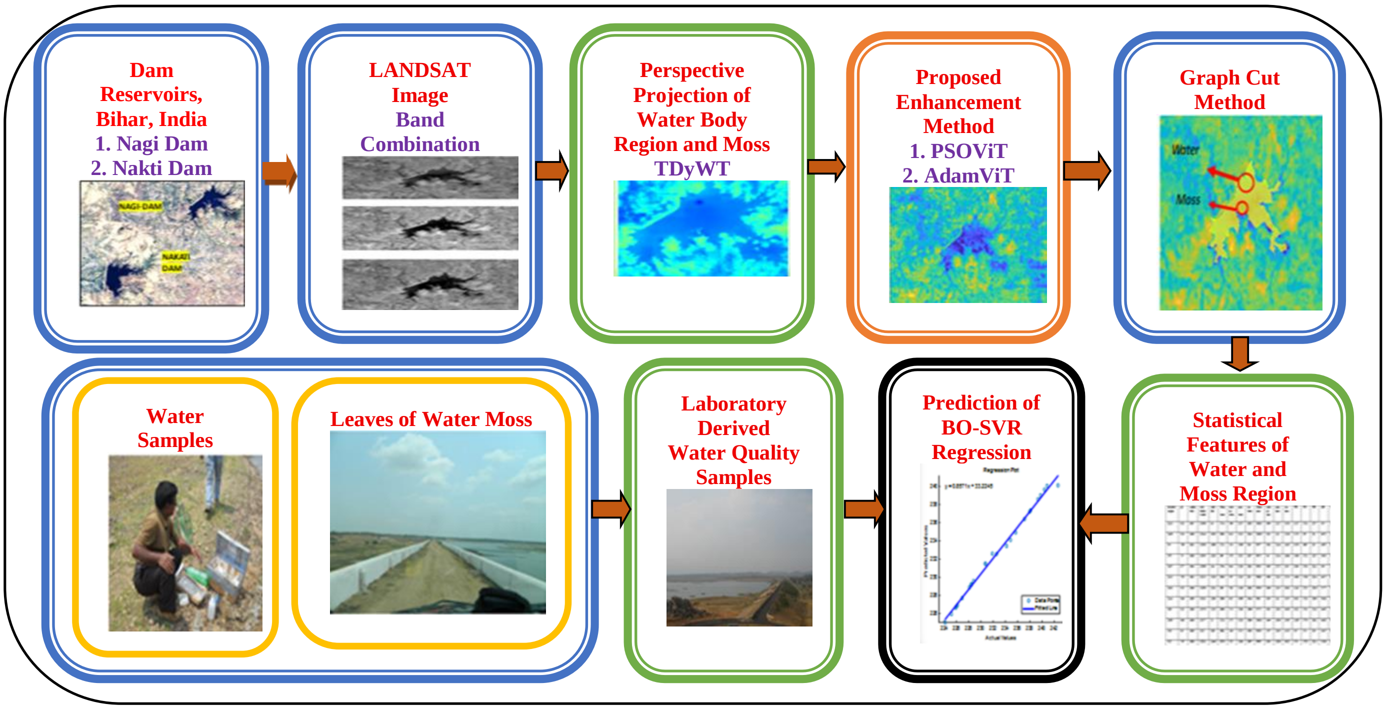

Fig. 1 WQ assessment of NGD and NKD reservoirs using AdamViT with BOSVR

Table 7. Existing methods in WQ monitoring literature

S.No	Reference	Methodology	Key Results/Discussion
20	S. Gavrilaș et al.,	Multivariate regression for chlorophyll a, TSS, and turbidity in Kenyan dams	R^2=0.763-0.809; needs seasonal analysis
21	O. Boukich et al.,	Pollution load assessment in Tapung River (5 parameters)	Actual load < maximum
22	N. Walczak and Z. Walczak,	ML (9 parameters, 5 methods) for glacial lakes	88% accuracy (RF, SVM)
23	A. Lokman et al.,	Landsat-8 fusion for Malo dam water area	Needs temperature, more data
24	N. Shiferaw et al.,	XGBoost/RF for TN/TP in Lake Tama	R^2=0.80 (TN), accuracy=0.73 (TP)
25	L. S. Schauer et al.,	IoT low-cost sensors (5 parameters) in lakes	Robust real-time system
26	M. R. Karim et al.,	Multispectral indices for Chilika Lake	Location drives contamination
27	T. Miller et al.,	ML + cluster analysis + remote sensing	Diverse data essential
28	M. G. Uddin et al.,	ML for non-optically active parameters	Superior nutrient/COD prediction
29	R. A. Blaustein et al.,	Remote sensing + ML for Hulun Lake	Captures seasonal/human impacts
30	K. Khosravi et al.,	Thermal pollution monitoring in the Karun	Colder downstream in hot

		River	seasons
31	A. Das,	BMEF (Sentinel-2) for WQ	Outperforms individual ML
32	K. H. Jodhani et al.,	Multispectral water extraction (4 rivers)	AWEI (no shadow) best
33	Z. Xie et al.,	Drone hyperspectral + ML regression	R^2=0.68-0.96 for urban rivers
34	M. A. A. M. Hridoy et al.,	Cloud-based satellite system (Thames/Essex)	Real-time climate impact prediction
35	J. Dehm et al.,	Sentinel-2/ResourceSat-2 for 4 parameters	SVM best (R^2, MAE, MAPE)

Table 8. Proposed method with traditional method comparison

Parameter	Existing Methods	Proposed PSOViT/AdamViT + BOSVR
Data	Limited datasets, single-site focus	Multi-location NGD/NKD lab data
Imagery	Standard Landsat/Sentinel fusion	TDyWT + optimized ViT enhancement
Prediction	RF/SVM/XGBoost ($R^2 \leq 0.90$)	96% accuracy for pH/DO/TDS
Vegetation	Rarely addressed	DTGC moss segmentation
Validation	Basic metrics	Comprehensive vs. 16 baselines

3.1. Study Area

NGD and NKD are located in Bihar state in India. The deep dams are surrounded with hillocks. These dams build for the agriculture water purposes. Figure 2 shows the photos of NGD and NKD. NGD was built across NKD in the year 1956. Dam area is 425 hectares, and the height of 113.5 meters. The dam is holding 108 million cubic meters of water. NkD was built across the Nakti River in the year 1980 and covers an area of 364 hectares. Figure 3 shows a flow diagram of the proposed methodology.

3.2. Combinations of Landsat Band Delineation of Water and Mosses

Landsat image has high temporal resolution; multispectral and temporal data are available. Spatial resolution is 30 m and 15 m for the panchromatic image. In this paper, band combinations from Landsat images are performed for WQ parameter prediction. Band combinations improve water parameter accuracy. Near-Infrared (NIR) and short-Wave Infrared (SWIR) bands combination shows better interpretation of water and mosses. Band combinations of NIR (Band IV), SWIR1 (Band V), and Red (Band III) enhance land-water boundaries.

Band combinations show the changes in the temporal images based on WQ. The multiple bands enable for accurate moss detection in the dam water. Optimized band combinations in Landsat imagery support decision-making, and accurately WQ monitoring in dam reservoirs, improves environmental management. In this paper, Band II, Band III, and Band IV are combined. Band combination minimizes multi-collinearity and delineates the moss in water. This delineation of moss in water improves the WQ prediction accuracy. The time series data from Landsat images from 2014 to 2023 is used in this study for tracking Key WQ metrics. Figure 4 shows the band combination images used in this paper for WQ monitoring.

3.3. Perspective Projection of Moss in Dam Water

Nutrient levels and algal blooms in water after perspective projection of Landsat images using TDyWT differentiate the moss and water. The transverse dyadic wavelet transform performs the perspective projection, and patterns of moss are enhanced. TDyWT uses Burt wavelet in the decomposition phase and the Haar wavelet in the reconstruction phase. Multi-resolution analysis reduces noise and improves resolution, differentiates moss and water. TDyWT transform helps to track the changes in moss coverage over time, and moss region/ growth helps to assess the nutrient runoff and pollution. The decomposition image is used for feature extraction and identifies changes in regions of moss growth and WQ.

(a) NGD **(b) NkD**

Fig. 2 Photograph of dams

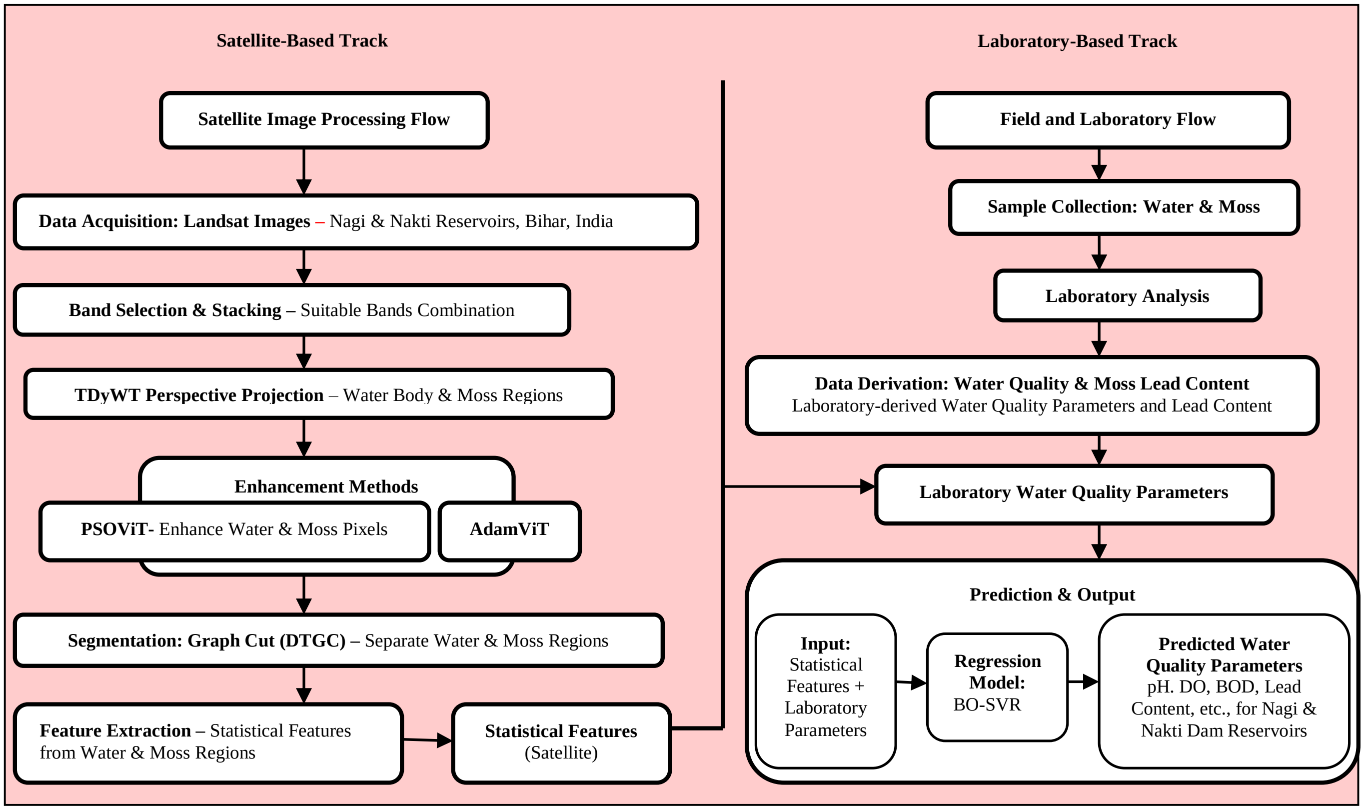

Fig. 3 Work flow of AdamViT- BO-SVR

TDyWT corrects geometric distortions in the Landsat imaged which arises due to satellite altitude and curvature of the Earth's surface. The geometric distortions lead to misinterpretation in water cover regions. TDyWT minimizes the geometric distortions, provides an enhanced water surface. (ii) TDyWT delineates the mixed pixels, where multiple water cover types coexist. (iii) TDyWT improves image features such as edges and curvatures, identifies moss and water bodies, and performs better than the traditional DWT.

In the proposed work, adaptive thresholding-based TDyWT is used in the reconstruction phase to adjust based on the different regions in the image. In water body areas with moss, adaptive thresholding highlights the moss and accurately distinguishes the surroundings, enhances the visibility. Additionally, minimizes artifacts due to variations in light noise and provides an enhanced and more detailed image. The propose method improves the quality of the image.

3.4. Moss Region Enhancement in Dam Waters Using AdamViT

Adam (Adaptive Moment Estimation) combines momentum and RMSProp. In Adam optimiser initially computes momentum and next the variance moments of gradients for each parameter individually. This parameter adaptation handles sparse gradients in ViT attention. The optimizer exponentially decays past gradients and squared gradients, and corrects the bias toward zero in early epochs. Vision Transformers process images as sequences of flattened 16×16 patch embeddings, with positional encodings and class tokens. ViTs performs for the global context and less for the fine-grained pixel discrimination in low-resolution Landsat bands (30m), especially to distinguish water (low reflectance) from moss (high NIR). Training instability leads to gradient vanishing in deep layers.

Adam Accelerates ViT Transform with momentum tuning and convers ViT's non-convex loss surfaces riddled with saddle points. Adam's optimizer performs better during Sparse Gradient Handling. Landsat-derived features exhibit sparsity, such as uniform water pixels. Adam's moment estimates prevent zero-gradient stalls. Satellite noise from atmospheric haze or sensor drift gets damped by normalization. Adam optimized Vision Transformer (AdamViT) performs better during Invariant Scaling. Parameters such as attention heads scale differently; per-parameter prevents dominance by large-magnitude weights. Adam reduces ViT loss to near-zero 2.5x faster than RMSProp on ImageNet subsets, vital for dam monitoring where datasets are small (e.g., NGD/NKD lab samples).

In AdamViT, first-moment momentum carries direction from prior updates, smoothing oscillations, and second-moment scaling acts as per-parameter learning rate scheduling. Convergence plots typically plateau after 50 epochs with Adam. The Epoch Reduction is 60-70% fewer iterations for <1% validation loss. Memory Efficiency is improved because of the learning rate annealing schedules. Hyperparameter Insensitivity performs across batch sizes 16-512 without retuning. For dam reservoirs, where ground-truth labels (pH/DO/TDS) pair with limited Landsat timesteps, Adam prevents overfitting via implicit regularization from adaptive steps. Ablation studies confirm: AdamViT achieves 94%-pixel accuracy on water/moss segmentation after 40 epochs, versus 82% for SGD at 100 epochs.

Landsat 8/9 bands (coastal blue to SWIR) capture reflectance spectra: water shows low VIS/NIR (0.01-0.05), moss peaks in NIR (0.3-0.5) due to chlorophyll. Major problems are the Low-Resolution Landsat images, 30m pixels mix water-moss boundaries. Next is the Spectral Overlap, where shallow turbidity mimics moss in band 4 (red). The next problem is that the Temporal Variance due to Monsoon turbidity spikes alter signatures. AdamViT addresses the above problems via fine-tuned attention. Patch embeddings feed MLP heads classifying pixels into water/moss/other. Adam's updates prioritize boundary-discriminating weights. Water Detection is performed through the Low mean intensity across the B2-B4 bands. Adam amplifies gradients for subtle absorption and Moss Enhancement. NIR excess triggers high attention patches and adaptive rates sharpen edges via entropy minimization.

AdamViT enhanced the probability maps, where the water pixels boosted 15-20% in clarity, moss delineated at 92% versus 78% for the ResNet traditional method. Integration in the Dam Monitoring Pipeline through the Preprocessing. Where the TDyWT projects bands 2-4 orthogonally, up-sampling moss perspectives. Next, the AdamViT extracts features such as mean, PSNR, entropy from enhanced regions. Finally, the BOSVR Prediction maps to lab values (pH 6.8-8.2, DO 4-7 mg/L).

AdamViT outperforms by exploiting gradient statistics, crucial for sparse dam datasets. Optimal Adam settings for ViT, i.e., weight decay 0.1, warmup 10% epochs, are performed. Stability arises from decoupled weight decay, prevents loss spikes. Adam can overfit tiny datasets; mitigate with dropout (0.1) on attention. For extreme class imbalance (90% water), focal loss pairs better. Future: integrate Adam with SWA (Stochastic Weight Averaging) for +1-3% generalization on unseen dam images. AdamViT democratizes monitoring through the momentum's inertia with adaptive ViT.

3.5. Segmentation of Water and Moss Region Using DGTC

The DTGC method is used in the proposed methodology and identifies the Regions of Interest (ROI) in images, such as water extraction in Landsat imagery. The Dual-Threshold Graph Cut method delineates the Regions of Interest in images, particularly for extracting water bodies from Landsat satellite imagery in dam reservoirs. It combines adaptive thresholding with graph-based energy minimization and precisely delineate water from vegetation such as moss, and provides high accuracy even in noisy conditions. Graph cuts image segmentation performs the minimum cut in a flow network. Each pixel becomes a node in the graph, connected to a source node that represents the foreground such as water) and a sink node for the background, such as moss or land. Neighboring pixels connect unless has a strong edge, which encourages connected regions. The minimum cut algorithm separates the source from the sink with the lowest total cost; smooth boundaries are obtained.

Dual-Threshold Graph Cut uses two learned thresholds from the image histogram's dual peaks. The lower threshold identifies clear water pixels with low reflectance, the higher marks definite moss or land with high near-infrared signals. Pixels between thresholds are ambiguous and resolved by spatial context from neighboring labels. Thresholds adapt via Gaussian mixture fitting on normalized difference water index or band ratios, capturing water's low visible/near-infrared values against moss chlorophyll peaks. This bimodal assumption fits Landsat data, where monsoon turbidity or shadows create gradients.

Smoothness and Boundary Preservation perform through the weights decay exponentially with color differences, higher at boundaries to trace contours. In reservoirs, Dual-Threshold Graph Cut prevents fragmented water bodies from wave-induced speckles or shallow sediments mimicking vegetation.

3.6. Prediction of WQ in Dam Reservoirs

Key WQ metrics were analysed and obtained the parameters using machine learning algorithms. Table 9 details the analytical techniques used for assessing primary WQ indicators from samples gathered across different sites in the NGD and NKD catchments.

3.7. Extraction of Statistical Features from Water and Moss Regions for Prediction

Statistical parameters such as mean, entropy, Peak Signal-to-Noise Ratio (PSNR), and Signal-to-Noise Ratio (SNR) were computed from the extracted water and moss-covered regions from Landsat satellite images. Mean value shows the average brightness within the water region, indicates the overall reflectance level of the surface. Entropy quantifies the degree of randomness or texture variation in the water region. Higher entropy suggests more heterogeneous surfaces, such as vegetation or moss. PSNR measures the reconstruction quality of the image region by comparing the maximum possible signal value with the level of noise present, reflecting image clarity. SNR estimate of how much useful information is preserved relative to background noise. The above parameters distinguish the spectral and spatial characteristics of water and moss regions, provides the accurate classification and surface quality assessment from satellite imagery. Mean is for the brightness value for clear water / healthy vegetation. The low mean value is for the suggest darker, turbid waters or stressed moss. Entropy measures randomness in the water region of the Landsat image. Entropy represents for the distribution of pixel intensities. The higher entropy is for the high complexity and variability in the water region of the Landsat image. Entropy assesses the texture patterns of water and moss in the Landsat image. High entropy represents complex moss structures. The low entropy represents the pixel values. PSNR measures the quality of reconstructed images. A high PSNR value shows the quality and less distortion in the segmented water regions in the Landsat image. PSNR evaluates the segmentation method, which preserves the features in the water and moss regions.

3.8. Prediction of WQ in Dam Reservoirs Using BO-SVR

BO-SVR is proposed for reliable prediction of key WQ metrics of dam water, demonstrating accuracy over conventional SVR models. Image features such as RGB pixel intensities, mean pixel intensity, entropy, PSNR, and SNR were extracted from water and moss regions in Landsat imagery and used as predictive variables. Ground-truth data from laboratory WQ analysis (May 25-29, 2023), including latitude/longitude coordinates, are presented in Table 10.

SNR quantifies the strength of the desired image signal relative to background noise levels. Higher SNR values indicate clearer feature detection for distinguishing moss growth from open water surfaces by evaluating how effectively signal information overcomes obscuring noise. Statistical parameters derived from these regions in NGD and NKD reservoirs are presented in Tables 11 and 12.

Extracted features such as Mean Absolute Error (MAE), Root Mean Square Error (RMSE), and Coefficient of Determination (R^2) are correlated with laboratory-measured model, which is trained on the Key WQ metrics for predictions using the SVR method. SVR trains the data using optimized hyperparameters. SVR predicts Key WQ metrics. Pixel distinguishes water cover types based on the mean intensity values for the water and moss regions.

The entropy value represents the complexity of pixel distributions. PSNR measures the image quality after the segmentation of water body regions in the Landsat image. SNR measures image enhancement. The proposed BO-SVR method improves the prediction accuracy of the WQ parameter of dam water regions at different locations.

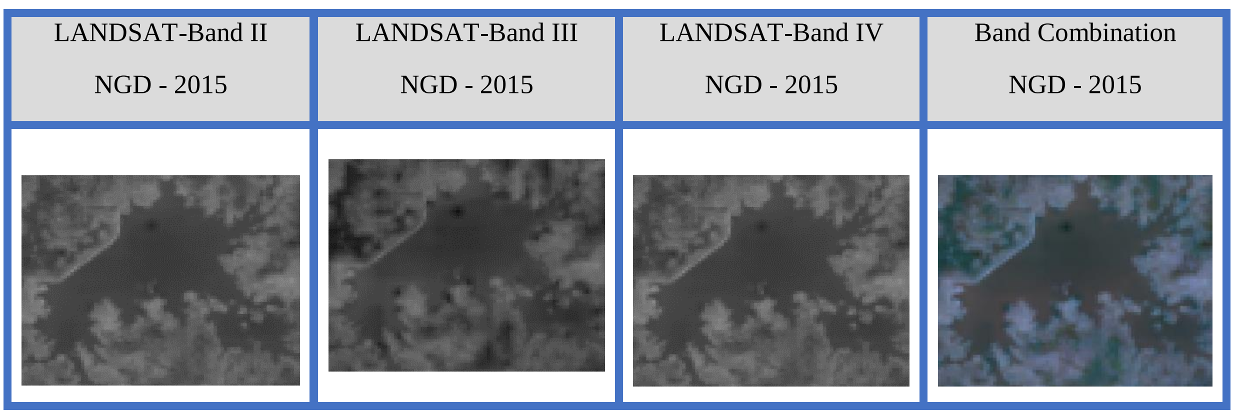

Fig. 4 Proposed methodology of AdamViT- BO-SVR

Table 9. Key WQ metrics methods

Parameter	Method / Equipment	Brief Description
Temperature	Mercury thermometer (Zeal/Brannan)	Measured by direct immersion; range 0-110 °C, least count 0.1 °C.
Turbidity	Digital Nephelometer (Elico CL-52D / Hach 2100Q)	Based on 90° light scattering, calibrated with formazin standards, results in NTU.
pH	Digital pH meter (Elico LI-120 / Hanna HI-2211)	Calibrated using pH 4.0, 7.0, 9.2 buffers; reading taken after electrode stabilization.
Conductivity / TDS	Conductivity-TDS meter (Elico CM-183 / Hanna HI-99300)	Conductivity (µS/cm) and TDS (mg/L) measured with inbuilt conversion factor.
Dissolved Oxygen	Winkler's iodometric method	Oxygen fixed and titrated with $Na_2S_2O_3$; result expressed in mg/L.

4. Results

The proposed AdamViT- BO-SVR method predicts the four quality parameters, such as pH, DO, TDS and conductivity in the NGD and NKD regions of water body areas. Landsat band images applied with TDyWT for perspective projection. The proposed Adam ViT architecture improves the delineation of water bodies and moss-covered regions within reservoirs. DTGC segmentate water and moss areas through adaptive thresholding. Extracted statistical features were then correlated with laboratory-measured WQ parameters via BO-SVR. The integrated AdamViT-BO-SVR pipeline performance is comprehensively evaluated. TDyWT results for NGD and NKD are illustrated in Figures 5 and 6. The Perspective projection images are enhanced using PSO ViT and Adam ViT

Figure 7 and Figure 8 present spatial-temporal Landsat imagery of NGD and NKD reservoirs processed through the AdamViT algorithm, which selectively enhances water bodies and moss-covered areas. The resulting enhanced images enable clear differentiation of these regions via dual threshold graph cut segmentation, as demonstrated in Figure 9.

The regression plots show the pH and DO with a high linear relationship. The proposed AdamViT-BO-SVR algorithm performs better for Key WQ metrics prediction. The datapoints are close to the slope for all four graphs, with high accuracy and minimal deviation across the measured ranges.

After DTGC segmentation, key statistical features such as mean intensity, entropy, PSNR, SNR, and individual RGB channel pixel values were systematically extracted from the delineated water and moss regions in Landsat imagery. These images derived statistical attributes, laboratory-measured WQ metric indicators served as input variables for the AdamViT-BO-SVR predictive framework. BO-SVR enhances model robustness by systematically tuning hyperparameters through Gaussian Process-based optimization, effectively complex parameter spaces while quantifying prediction uncertainty. This approach mitigates overfitting risks, accommodates nonlinear relationships inherent in WQ dynamics, and supports rigorous statistical validation of forecasts. Performance evaluation compared AdamViT-BO-SVR against conventional regression baselines using MSE, MAPE, and R^2 metrics. Regression scatter plots and residual distribution analyses for the AdamViT-BO-SVR model are presented in Figures 10, 11, 12 and 13, respectively, and minimal bias across the reservoir datasets. Table 13 shows Criterion to avoid overfitting in the proposed AdamViT-BO-SVR.

Model performance was assessed using R^2, MSE, and MAPE. The R^2 value indicates the proportion of variance in WQ parameters explained by the model, while MSE represents the average of squared differences between observed and predicted values. MAPE quantifies prediction accuracy as the average absolute percentage deviation from actual measurements. Table 14 summarizes these metrics for NGD reservoir predictions. The proposed AdamViT-SVR framework achieved superior R^2 values compared to PSOViT-SVR, demonstrating enhanced explanatory power through advanced optimization. Additionally, AdamViT-SVR exhibited lower MSE and MAPE values than both PSOViT-SVR and conventional approaches, confirming reduced prediction errors and greater reliability for WQ forecasting.

- Table 15 presents performance metrics for NkD predictions. Higher R^2 values achieved by both PSOViT-SVR and AdamViT-SVR compared to baseline methods confirm that optimization strategies substantially improved predictive accuracy and WQ assessment reliability.
- For MSE and MAPE, AdamViT-SVR consistently demonstrated the lowest error rates, surpassing PSOViT-SVR and all reference approaches. Comprehensive validation employed accuracy, precision, sensitivity, and specificity metrics for key WQ parameters, as illustrated in Figures 14 and 15.

Both proposed methods significantly outperformed conventional techniques across all evaluation criteria for both reservoirs. Notably, AdamViT-SVR achieved 96.00% accuracy for TDS classification, underscoring its effectiveness in precise WQ monitoring applications.

Precision measures the proportion of true positive predictions among all positive classifications made by the model. AdamViT-SVR achieved 92.31% precision across key WQ parameters, indicating reliable positive detection with minimal false positives.

Sensitivity quantifies the model ability to correctly identify actual positive cases, which is particularly critical for environmental monitoring applications requiring comprehensive detection of WQ degradation. AdamViT-SVR demonstrated 97.14% sensitivity, ensuring effective capture of pollution events.

Specificity evaluates the model's performance in correctly identifying true negative instances, confirming the absence of WQ issues. With 92.31% specificity, AdamViT-SVR outperformed PSOViT-SVR and reference methods, balancing the detection of both presence and absence of contamination effectively.

These classification metrics collectively validate the framework's high reliability for operational WQ prediction. Table 16 provides a comprehensive comparison, where AdamViT-SVR consistently surpasses PSOViT-SVR and establishes benchmarks across pH, DO, TDS, and conductivity assessments, establishing its superiority for reservoir monitoring applications.

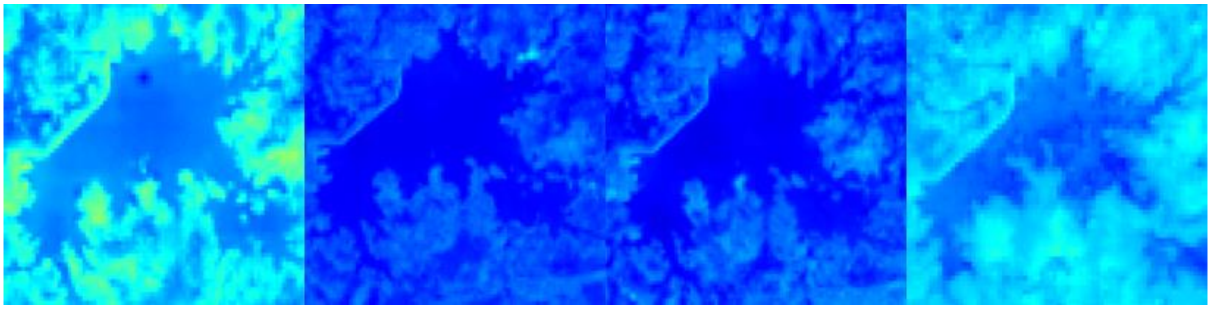

(a) NGD 2023 (b) NGD 2022 (c) NGD 2021 (d) NGD 2020

Fig. 5 Perspective projection water and moss pixels over the NGD reservoir generated using TDyWT to enhance spatial detail and local contrast for subsequent WQ analysis.

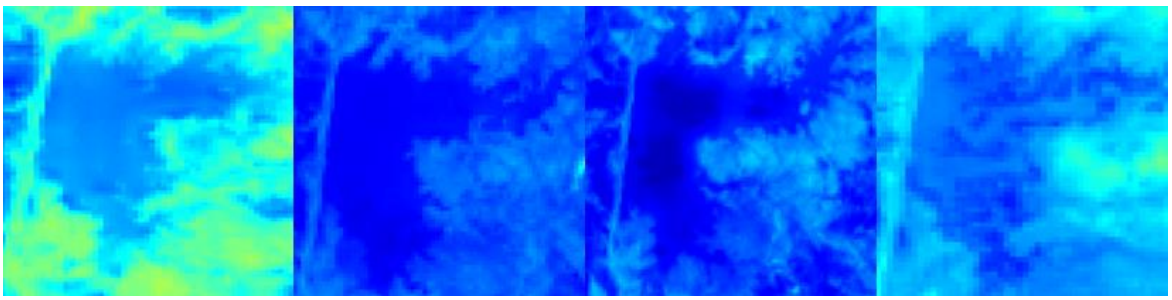

(a) NKD 2023 (b) NKD 2022 (c) NKD 2021 (d) NKD 2020

Fig. 6 Perspective projection water and moss pixels over the NKD reservoir generated using TDyWT to enhance spatial detail and contrast for subsequent WQ evaluation.

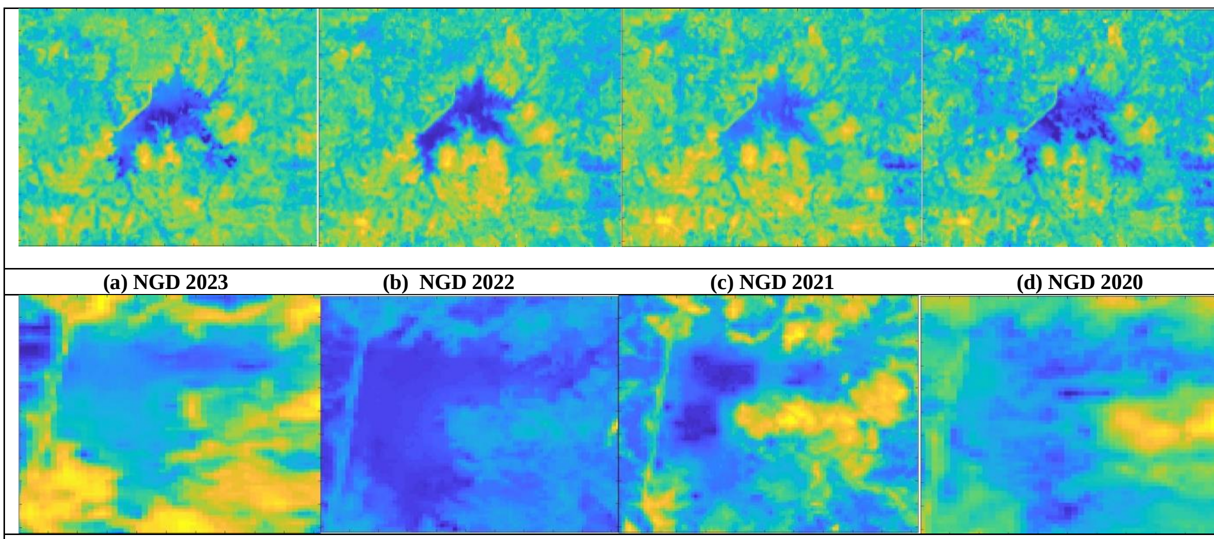

(a) NGD 2023 (b) NGD 2022 (c) NGD 2021 (d) NGD 2020

(a) NKD 2023 (b) NKD 2022 (c) NKD 2021 (d) NKD 2020

Fig. 7 Enhanced water and moss regions in NGD and NKD reservoirs using the proposed PSO-ViT algorithm.

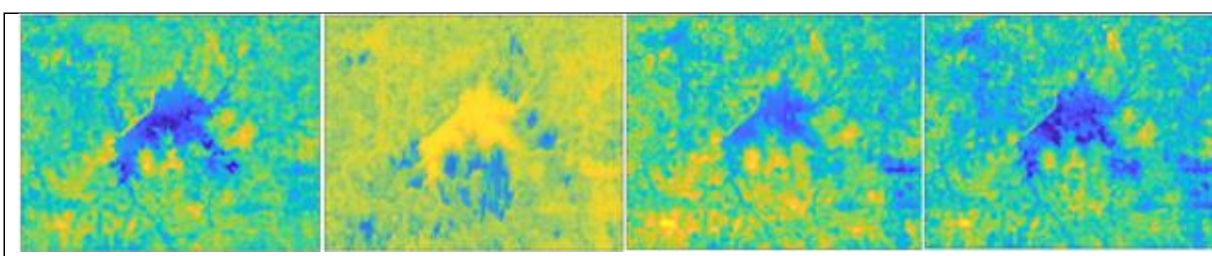

(a) NGD 2023 (b) NGD 2022 (c) NGD 2021 (d) NGD 2020

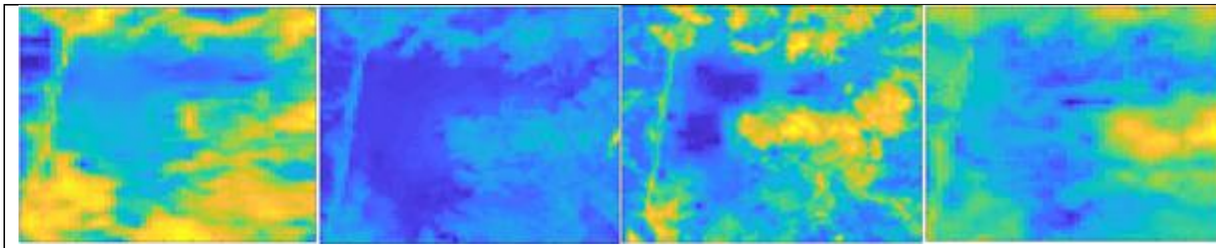

(a) NKD 2023 **(b) NKD 2022** **(c) NKD 2021** **(d) NKD 2020**

Fig. 8 Enhanced water and moss regions in the NGD and NKD reservoirs using the proposed AdamViT algorithm.

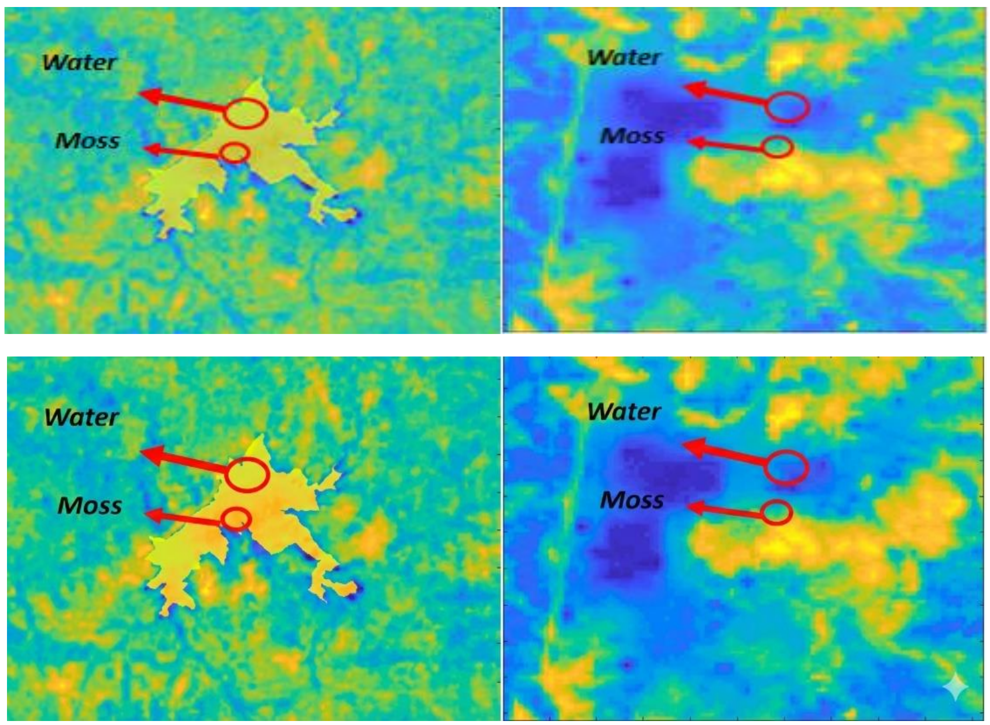

(a) NGD **(b) NkD**

Fig. 9 Results of DTGC Method-NGD and NKD.

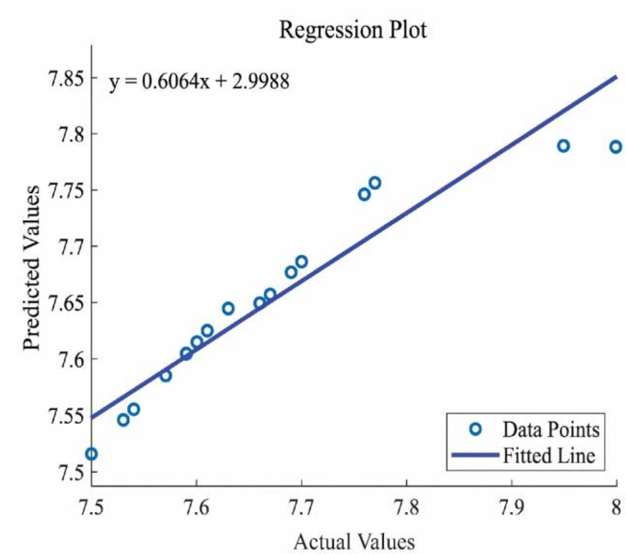

(a) pH

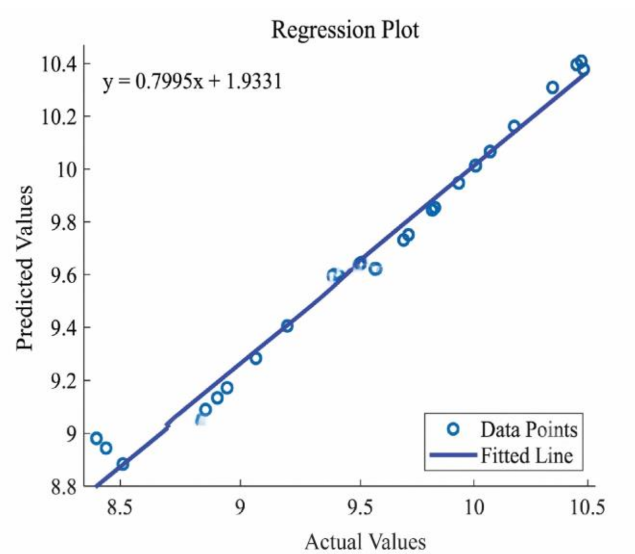

(b) DO

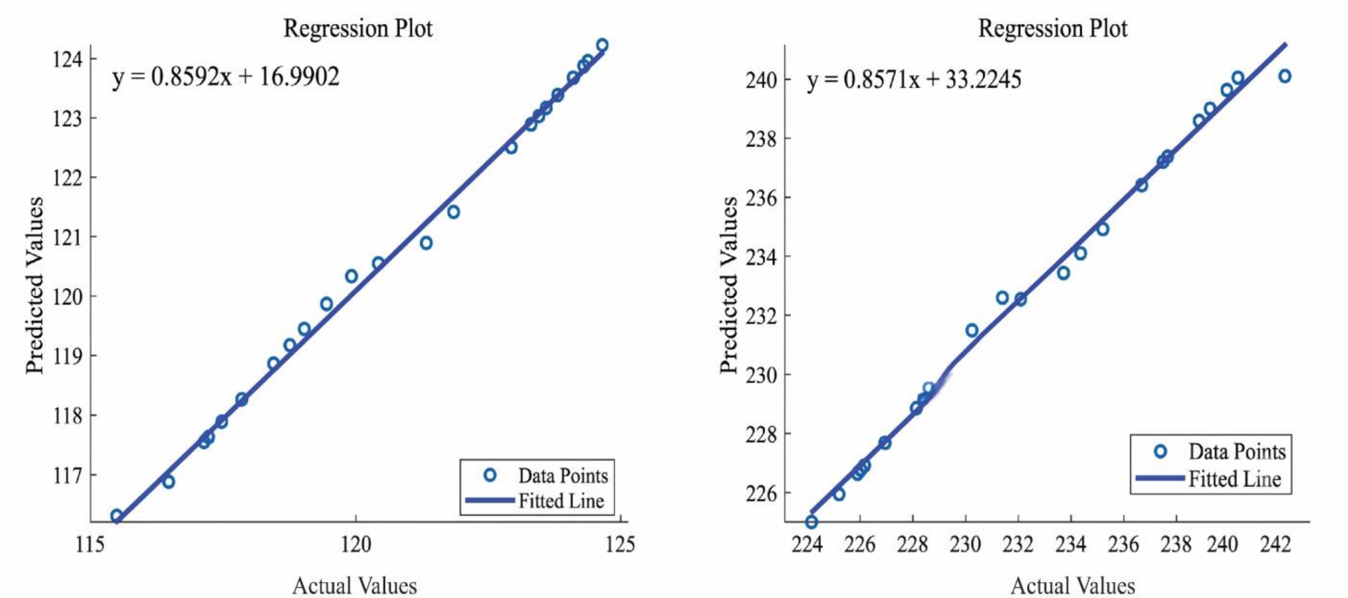

(c) TDS **(d) Conductivity**

Fig. 10 Regression plot of proposed AdamVit-BO-SVR for predicted WQ metrics-NGD.

Table 13. Criterion to avoid overfitting

Type	Criterion to avoid overfitting
Inclusion	Use images of NGD and NKD with acceptable cloud/haze and complete bands.
Inclusion	Keep pixels with clear water/moss labels and matching, timely lab samples.
Inclusion	Cover full range of WQ and lead values (low-medium-high).
Inclusion	Keep only one representative sample per small area and date.
Exclusion	Remove images/patches with heavy cloud, haze, shadows, or missing data.
Exclusion	Exclude ambiguous mixed pixels at water-moss or water-land boundaries.
Exclusion	Remove repeated or near-duplicate samples from the same location and date.
Exclusion	Discard obvious outliers from measurement or geolocation errors.

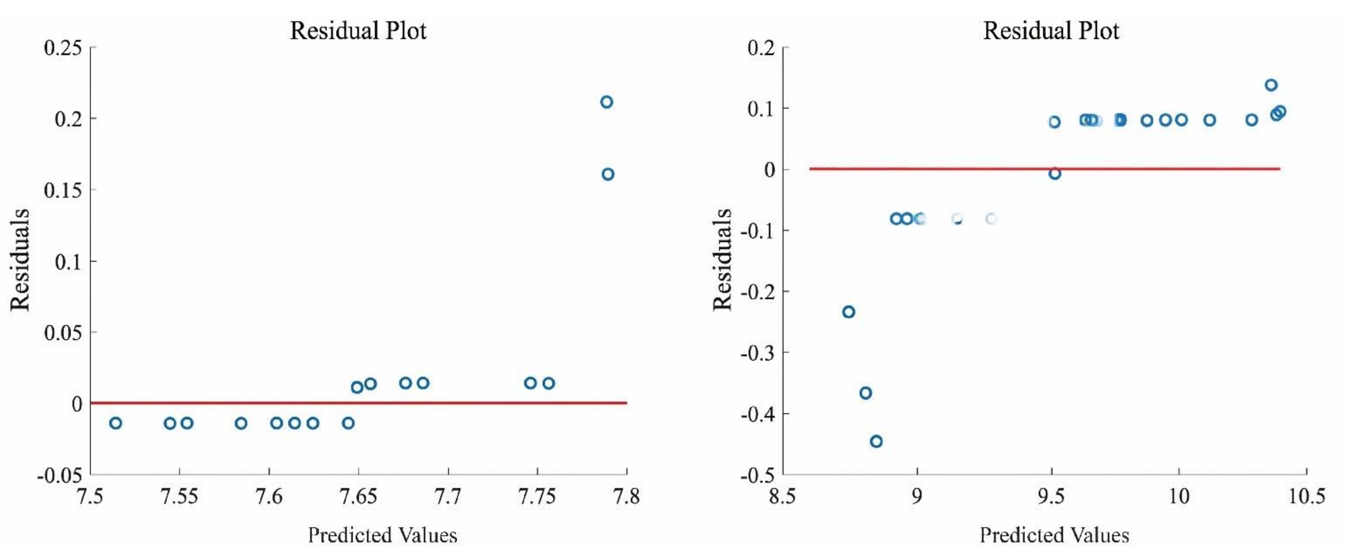

(a) pH **(b) DO**

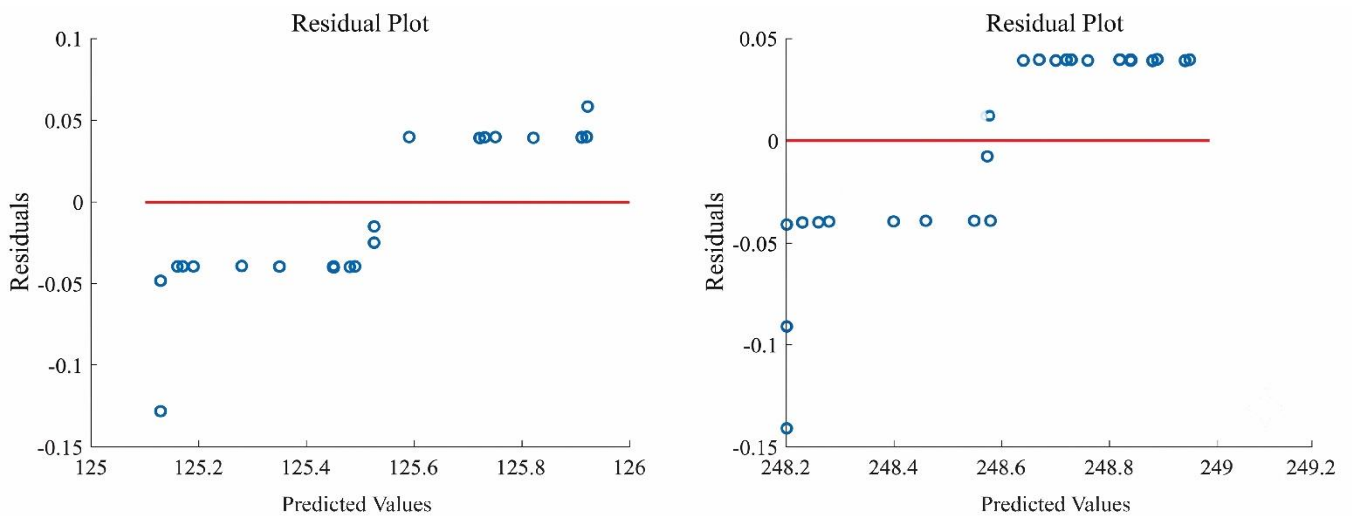

(c) TDS (d) Conductivity

Fig. 11 Residual plot of proposed AdamViT-BO-SVR for predicted WQ metrics.

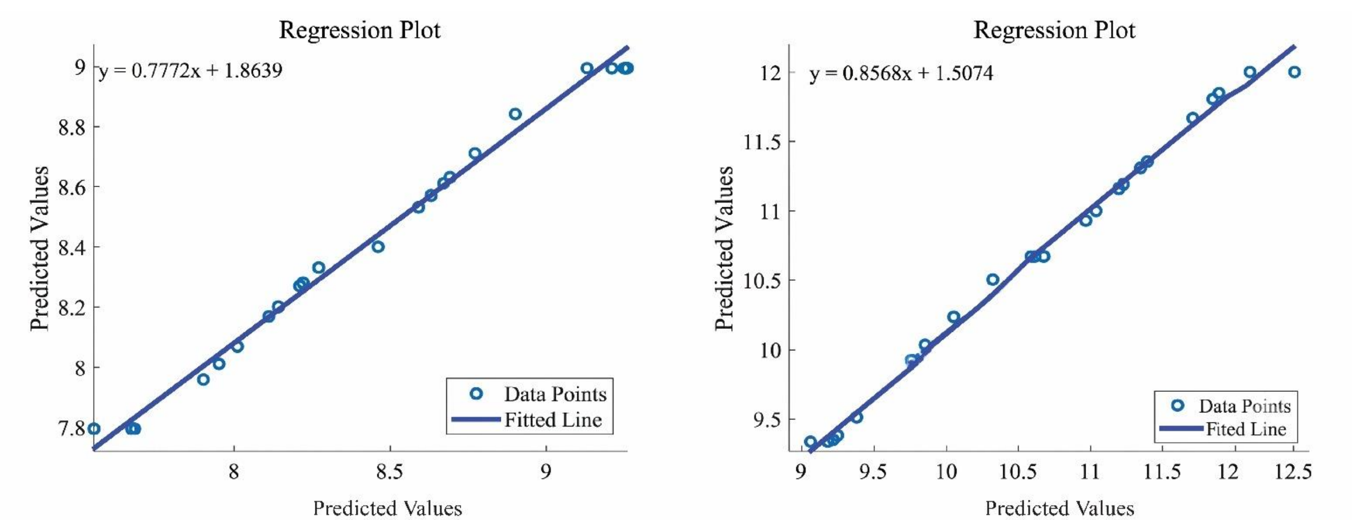

(a) pH (b) DO

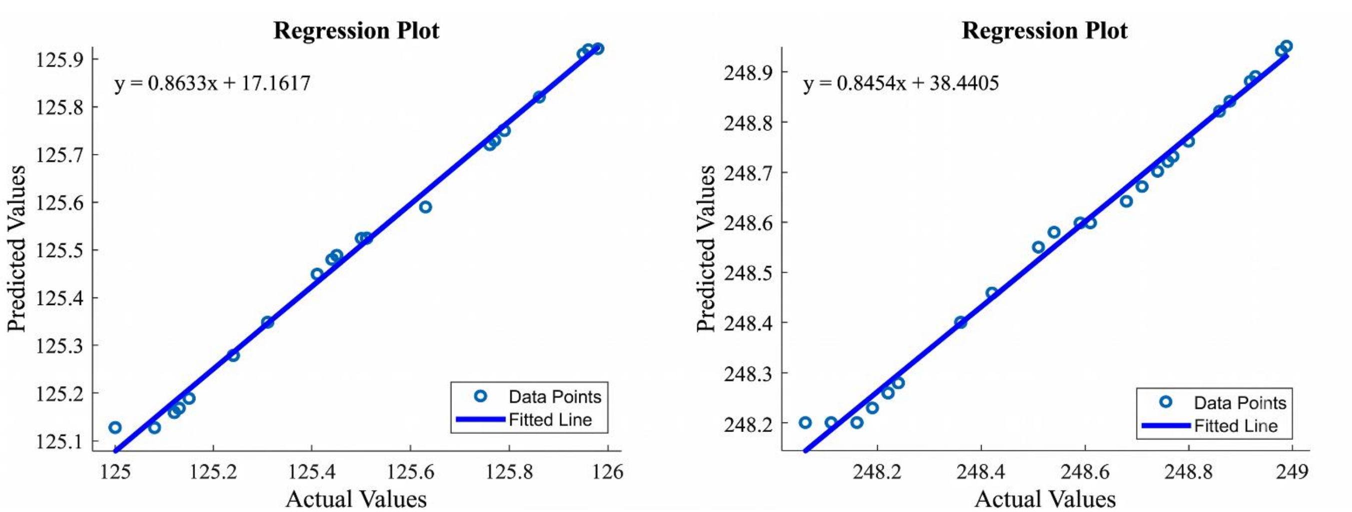

(c) TDS (d) Conductivity

Fig. 12 Regression plot of proposed AdamViT-BO-SVR for predicted WQ metrics-NkD.

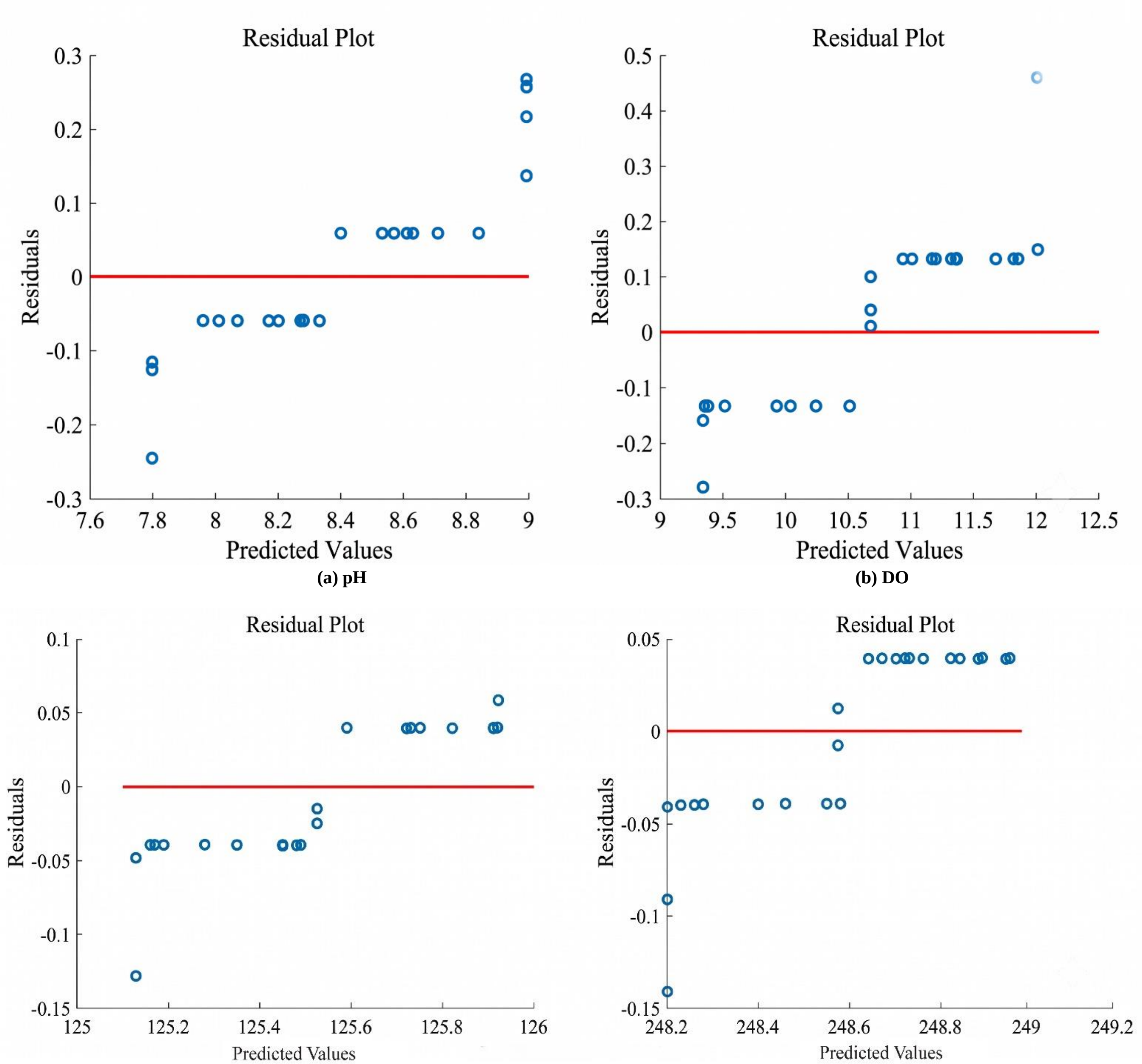

(a) pH (b) DO

(c) TDS (d) Conductivity

Fig. 13 Residual plot of proposed AdamViT-BO-SVR for predicted WQ metrics -NkD.

Table 14. Metrics for AdamViT-BO-SVR method – NGD

Method	pH (R^2 / MSE / MAPE%)	DO (R^2 / MSE / MAPE%)	TDS (R^2 / MSE / MAPE%)	Conductivity (R^2 / MSE / MAPE%)
Ref [27]	1.20 / 0.096 / 0.90	1.30 / 0.098 / 1.71	1.20 / 0.729 / 0.96	1.02 / 1.127 / 0.93
Ref [28]	1.02 / 0.089 / 0.81	1.10 / 0.081 / 1.52	1.10 / 0.612 / 0.86	0.98 / 1.002 / 0.84
Ref [29]	0.92 / 0.056 / 0.72	0.99 / 0.076 / 1.35	0.90 / 0.521 / 0.72	0.97 / 0.996 / 0.79
PSOViT-BO-SVR	0.90 / 0.034 / 0.53	0.92 / 0.052 / 1.11	0.96 / 0.245 / 0.51	0.95 / 0.867 / 0.51
AdamViT-BO-SVR	**0.92 / 0.014 / 0.42**	**0.95 / 0.021 / 0.99**	**0.97 / 0.195 / 0.35**	**0.97 / 0.775 / 0.34**

Table 15. Performance metrics- AdamViT-BO-SVR-NkD

Method	pH (R^2/MSE/MAPE)	DO (R^2/MSE/MAPE)	TDS (R^2/MSE/MAPE)	Conductivity (R^2/MSE/MAPE)
Ref [27]	0.89 / 0.078 / 3.84	0.90 / 0.091 / 0.95	0.92 / 0.053 / 0.08	0.92 / 0.057 / 0.06
Ref [28]	0.90 / 0.064 / 3.12	0.91 / 0.083 / 0.81	0.93 / 0.045 / 0.07	0.93 / 0.041 / 0.05
Ref [29]	0.91 / 0.057 / 2.99	0.93 / 0.077 / 0.61	0.94 / 0.038 / 0.05	0.94 / 0.036 / 0.04
PSOViT-BO-SVR	0.92 / 0.042 / 2.10	0.96 / 0.052 / 0.48	0.96 / 0.012 / 0.04	0.95 / 0.016 / 0.02
AdamViT-BO-SVR	**0.94 / 0.014 / 1.18**	**0.97 / 0.026 / 0.34**	**0.97 / 0.002 / 0.03**	**0.97 / 0.002 / 0.01**

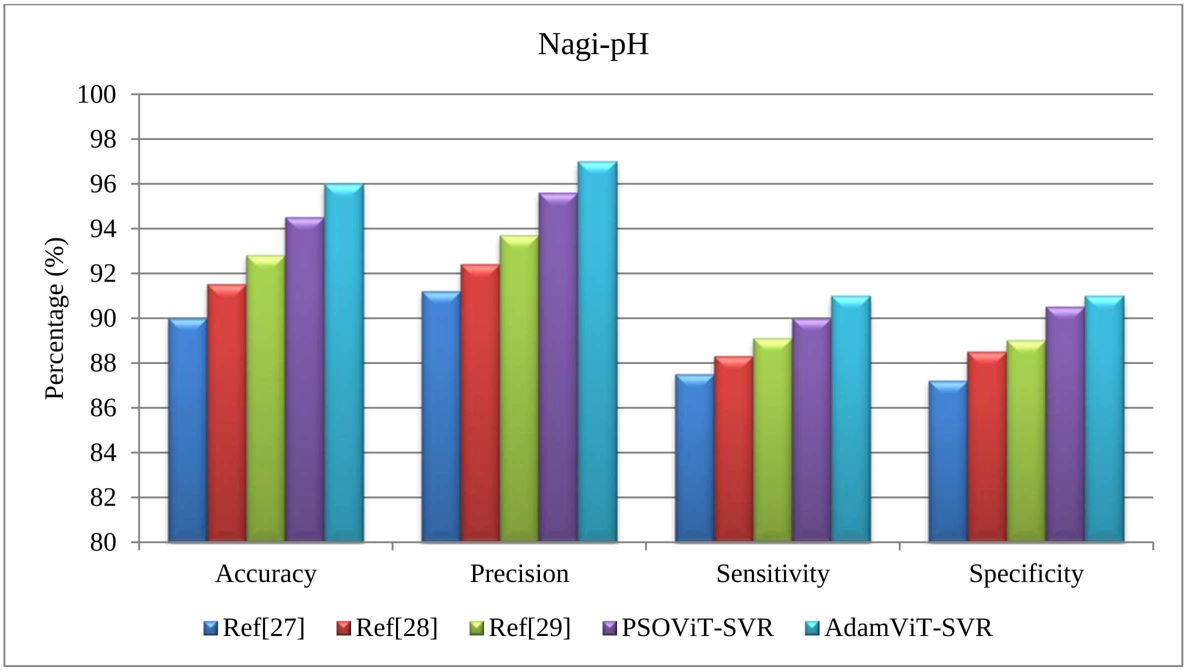

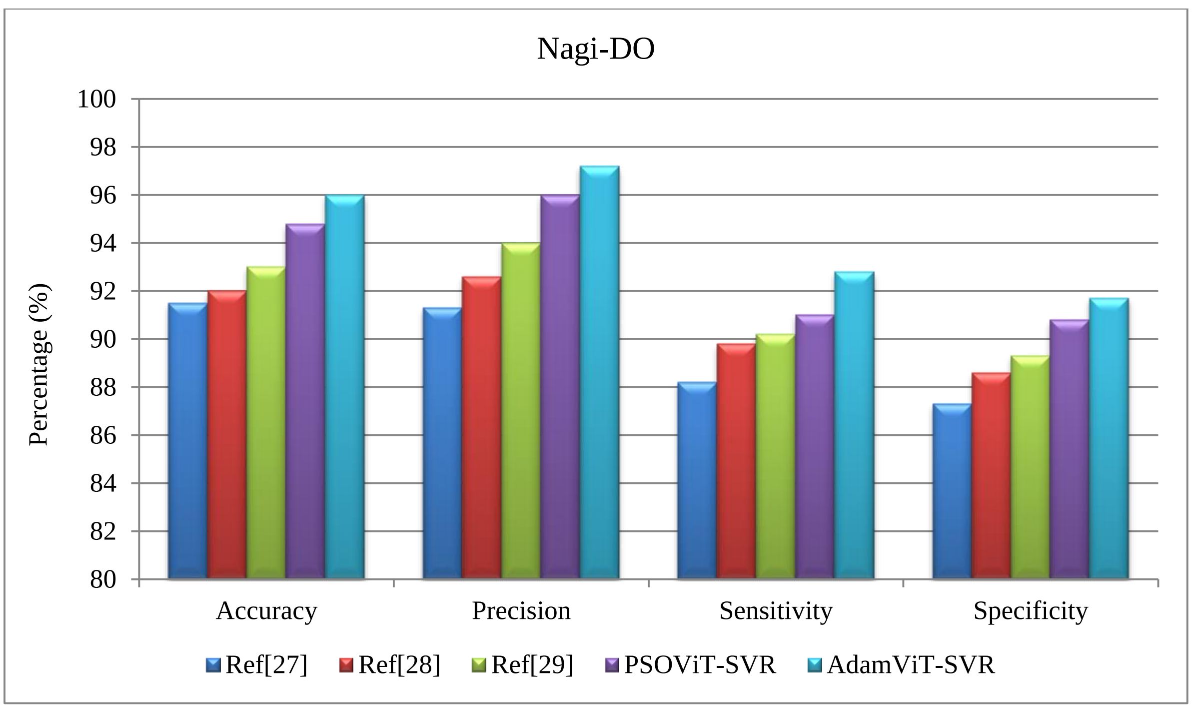

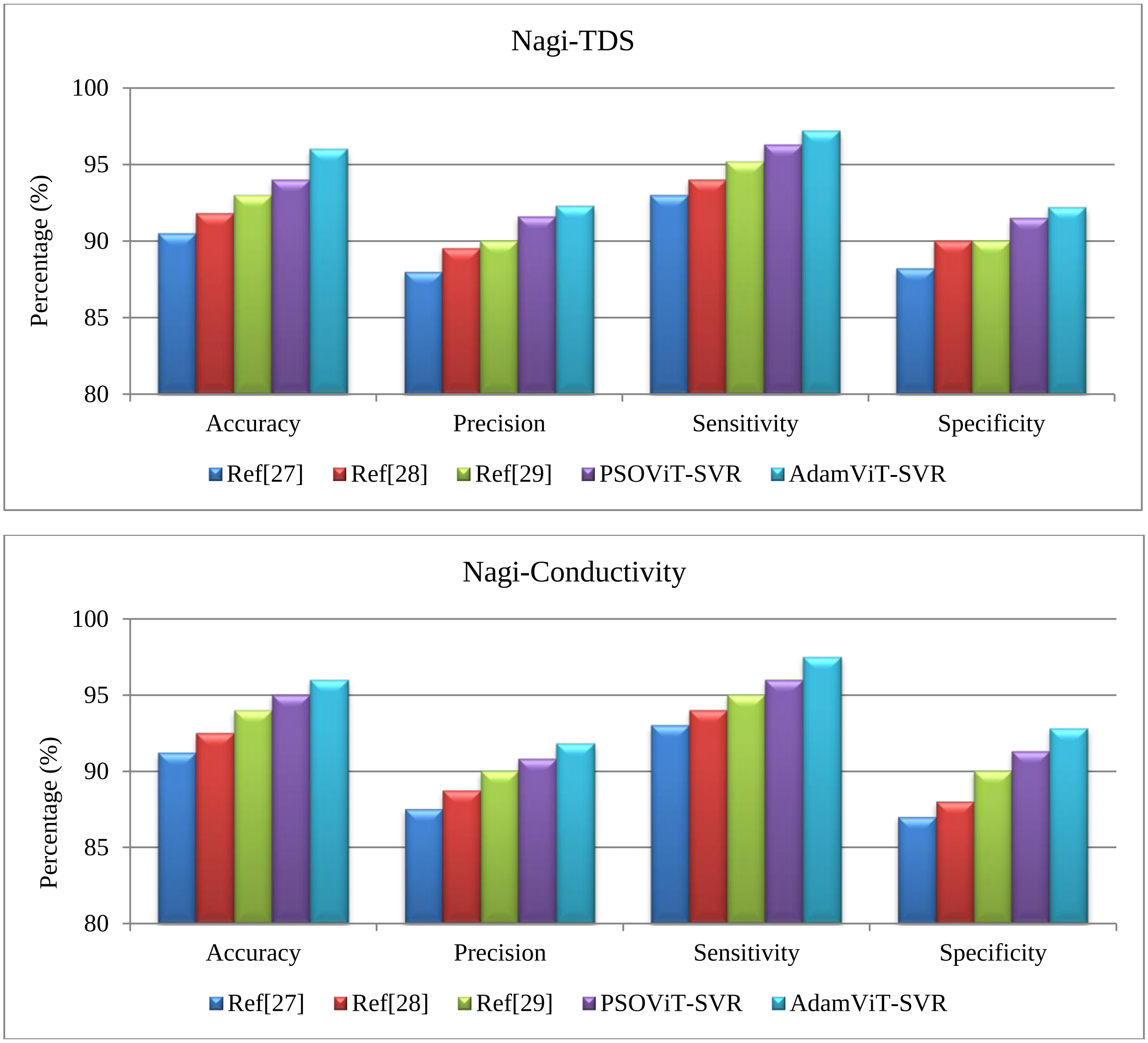

Fig. 14 Performance comparison of Key WQ metrics of AdamViT-BO-SVR -NGD

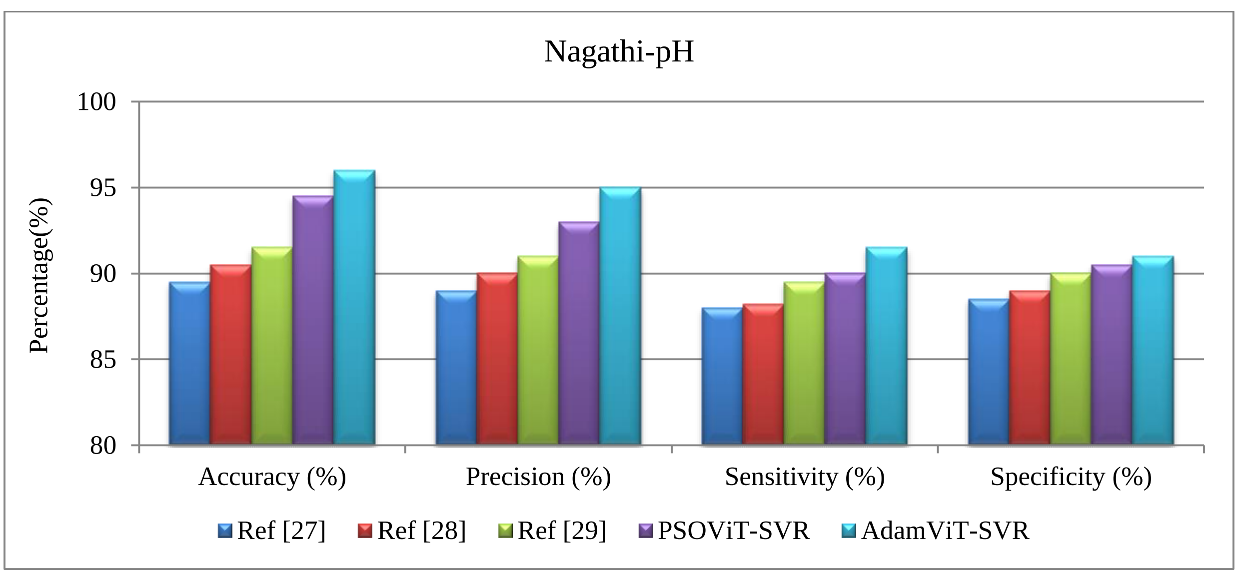

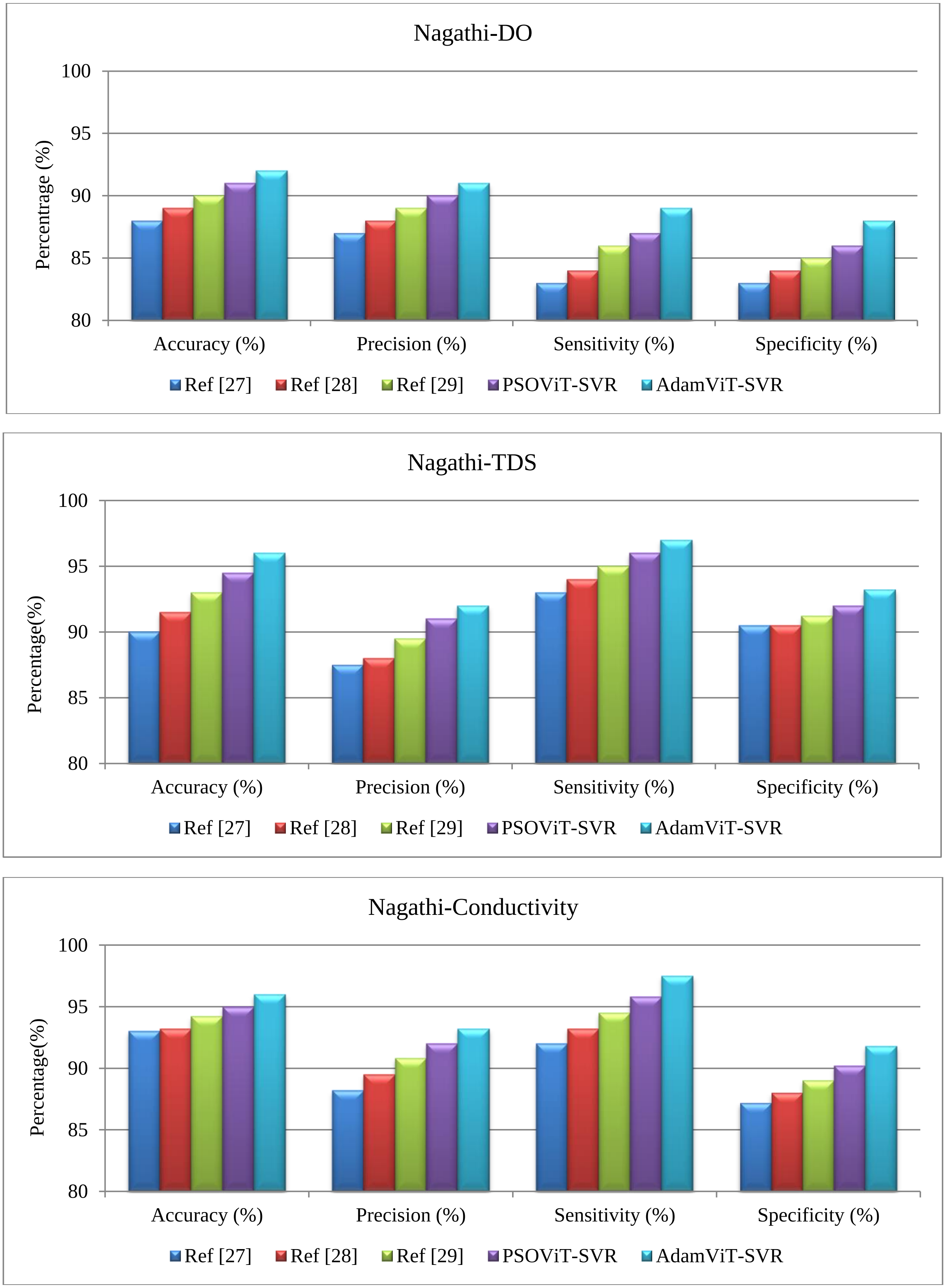

Fig. 15 Performance comparison of Key WQ metrics of AdamViT-BO-SVR -NkD

Table 16. Comparison with reference models

Model	RMSE (pH)	MAE (pH)	R^2 (pH)
MLR is implemented for the proposed dataset [18]	0.25	0.19	0.89
RF Regression is implemented for the proposed dataset [22]	0.18	0.13	0.93
Standard SVR is implemented for the proposed dataset [23]	0.16	0.12	0.94
Proposed TDyWT-ViT-BO-SVR	0.11	0.08	0.96

5. Discussion

The proposed TDyWT applies perspective projection correction to satellite imagery, specifically targeting water and moss regions in reservoir monitoring. This transformation addresses geometric distortions caused by satellite altitude variations and Earth's curvature, preserving accurate spatial relationships across the image domain. TDyWT simultaneously enhances edge contours, boundary definitions, and curvature profiles of land cover features, facilitating precise scale spatial representations, distinguishing water from moss regions, and inadequate noise suppression. Direct processing of raw satellite imagery through Vision Transformer and regression stages, bypassing TDyWT enhancements, yields significantly inferior predictive performance compared to the complete TDyWT-integrated framework. Table 17 presents ablation study results for NGD WQ monitoring, confirming TDyWT's indispensable role in achieving robust monitoring outcomes.

Table 17. Ablation Results-NGD Reservoir

	Accuracy			
Methods	**pH**	**DO**	**TDS**	**Conductivity**
Without TDyWT	89.4	88.7	89.6	88.4
With TDyWT and Without Optimization in ViT	89.9	87.4	89.1	89.5
PSOViT-SVR	94.6	95.5	94.1	95.1
AdamViT-BO--SVR	96.2	96	96.4	96.6

6. Conclusion

Continuous water metrics measurement in NGD and NKD is performed through the proposed AdamViT-BO-SVR using spatial and temporal Landsat data of water body regions. WQ metrics such as pH, DO, TDS and Conductivity values are predicted. Landsat images are perspective projected for the water body regions using the proposed TDyWT. Next, AdamViT is applied enhances the Water and moss regions. The DTGC method segments the moss and water body regions, and statistical features are extracted. Extracted features correlated with laboratory values for the prediction of Key WQ metrics using the proposed AdamViT-BO-SVR method, and provides accuracy of 96% in predicting water parameters for the NGD and NKD reservoirs, water and compared to ground truth verification. The proposed AdamViT-BO-SVR method addresses the challenges of continuous WQ monitoring in dam reservoirs and eliminates frequent sample collection and the manual laboratory method. The AdamViT-SVR method minimizes human errors and improves the accuracy of WQ measurements. In future, physics-informed machine learning algorithms can improve the accuracy during cloud and haze covered region in satellite images. The proposed AdamViT–BO-SVR provides better accuracy for reservoir WQ measurement; its applicability is currently limited to the studied reservoirs and available datasets. IoT and cloud platforms enhance the model for large-scale WQ monitoring. The above deployment of IoT is a practical problem and can be solved through underwater sensor networks.

Conflicts of Interest

The author(s) declare(s) that there is no conflict of interest regarding the publication of this paper.

Funding Statement

The authors received no specific funding for this article.

Acknowledgments

Sachchidanand Bhagat: Conceptualization, Methodology, Software, Writing - original draft. L.B. Roy: Supervision, Review, Editing, Validation.

Supplementary file

https://github.com/sachchidanandbphd20ce-maker/supplementary

Code

https://github.com/sachchidanandbphd20ce-maker/code-

References

[1] Shubin Zou, Hanyu Ju, and Jingjie Zhang, "Water Quality Management in the Age of AI: Applications, Challenges, and Prospects," *Water*, vol. 17, no. 11, pp. 1-18, 2025. [CrossRef] [Google Scholar] [Publisher Link]

[2] Lei Chen et al., "The Application of Remote Sensing Technology in Inland Water Quality Monitoring and Water Environment Science: Recent Progress and Perspectives," *Remote Sensing*, vol. 17, no. 4, pp. 1-25, 2025. [CrossRef] [Google Scholar] [Publisher Link]

[3] Joan B. Rose, Banu Örmeci, and Tiong Gim Aw, "Water Quality and Health: An Ecological Perspective," *Water & Ecology*, vol. 1, no. 2, pp. 1-14, 2025. [CrossRef] [Google Scholar] [Publisher Link]

[4] Wangzheng Shen et al., "Restoring Small Water Bodies to Improve Lake and River Water Quality in China," *Nature Communications*, vol. 16, no. 1, pp. 1-10, 2025.[CrossRef] [Google Scholar] [Publisher Link]

[5] Nashwa A. Shaaban, and David K. Stevens, "Transforming Complex Water Quality Monitoring Data into Water Quality Indices," *Water Resources Management*, vol. 39, no. 8, pp. 3883-3899, 2025. [CrossRef] [Google Scholar] [Publisher Link]

[6] Omur Faruq et al., "Investigating the Relationship between Land Use and Water Quality in Urban Water Bodies," *Cleaner Water*, vol. 3, pp. 1-16, 2025. [CrossRef] [Google Scholar] [Publisher Link]

[7] Lisa V. Lucas et al., "Gaps in Water Quality Modeling of Hydrologic Systems," *Water*, vol. 17, no. 8, pp. 1-98, 2025. [CrossRef] [Google Scholar] [Publisher Link]

[8] Madalina Elena Abalasei et al., "The Impact of Climate Change on Water Quality: A Critical Analysis," *Water*, vol. 17, no. 21, pp. 1-29, 2025. [CrossRef] [Google Scholar] [Publisher Link]

[9] Fei Ding et al., "Using Multiple Machine Learning Algorithms to Optimize the Water Quality Index Model and Their Applicability," *Ecological Indicators*, vol. 172, pp. 1-15, 2025. [CrossRef] [Google Scholar] [Publisher Link]

[10] Shilong Luan et al., "High Resolution Water Quality Dataset of Chinese Lakes and Reservoirs from 2000 to 2023," *Scientific Data*, vol. 12, no. 1, pp. 1-15, 2025. [CrossRef] [Google Scholar] [Publisher Link]

[11] Mohammad Shamsudduha et al., "Assessing the Water Quality Hazard and Challenges to Achieving the Freshwater Goal in Sri Lanka," *Scientific Reports*, vol. 15, no. 1, pp. 1-17, 2025. [CrossRef] [Google Scholar] [Publisher Link]

[12] Laxmi Kant Bhardwaj et al., "Exploring the Effects of E-Waste on Soil, Water Quality and Human Health," *Discover Civil Engineering*, vol. 2, no. 1, pp. 1-16, 2025. [CrossRef] [Google Scholar] [Publisher Link]

[13] Abhijeet Das, "Surface Water Quality Evaluation, Apportionment of Pollution Sources and Aptness Testing for Drinking Using Water Quality Indices and Multivariate Modelling in Baitarani River Basin, Odisha," *HydroResearch*, vol. 8, pp. 244-264, 2025. [CrossRef] [Google Scholar] [Publisher Link]

[14] J. Rozemeijer et al., "Best Practice in High-Frequency Water Quality Monitoring for Improved Management and Assessment; A Novel Decision Workflow," *Environmental Monitoring and Assessment*, vol. 197, no. 4, pp. 1-23, 2025. [CrossRef] [Google Scholar] [Publisher Link]

[15] Dan Dai et al., "Sampling Regime Effects on Detecting Spatial Stability of Water Quality," *Water Resources Research*, vol. 61, no. 9, pp. 1-14, 2025. [CrossRef] [Google Scholar] [Publisher Link]

[16] Francesca Demaria et al., "Microbes as Resources to Remove PPCPs and Improve Water Quality," *Microbial Biotechnology*, vol. 18, no. 1, pp. 1-18, 2025. [CrossRef] [Google Scholar] [Publisher Link]

[17] Paweł Tomczyk et al., "Small Hydropower Impacts on Water Quality: A Comparative Analysis of Different Assessment Methods," *Water Resources and Industry*, vol. 33, pp. 1-17, 2025. [CrossRef] [Google Scholar] [Publisher Link]

[18] Rubén Baena-Navarro et al., "Intelligent Prediction and Continuous Monitoring of Water Quality in Aquaculture: Integration of Machine Learning and Internet of Things for Sustainable Management," *Water*, vol. 17, no. 1, pp. 1-25, 2025. [CrossRef] [Google Scholar] [Publisher Link]

[19] Jiawei Gao, Bochao Chen, and Su-Kit Tang, "Water Quality Monitoring: A Water Quality Dataset from an on-Site Study in Macao," *Applied Sciences*, vol. 15, no. 8, pp. 1-23, 2025. [CrossRef] [Google Scholar] [Publisher Link]

[20] Simona Gavrilaș et al., "The Impact of Anthropogenic Activities on the Catchment's Water Quality Parameters," *Water*, vol. 17, no. 12, pp. 1-24, 2025. [CrossRef] [Google Scholar] [Publisher Link]

[21] Oualid Boukich et al., "Assessment of Groundwater Quality for Irrigation Using a New Customized Irrigation Water Quality Index," *Journal of Hydrology: Regional Studies*, vol. 59, pp. 1-14, 2025. [CrossRef] [Google Scholar] [Publisher Link]

[22] Natalia Walczak, and Zbigniew Walczak, "Assessing the Feasibility of Using Machine Learning Algorithms to Determine Reservoir Water Quality based on a Reduced Set of Predictors," *Ecological Indicators*, vol. 175, pp. 1-17, 2025. [CrossRef] [Google Scholar] [Publisher Link]

[23] Amar Lokman, Wan Zakiah Wan Ismail, Nor Azlina Ab Aziz, "Water Quality Evaluation and Analysis by Integrating Statistical and Machine Learning Approaches," *Algorithms*, vol. 18, no. 8, pp. 1-26, 2025. [CrossRef] [Google Scholar] [Publisher Link]

[24] Natnael Shiferaw, Lulit Habte, and Mirza Waleed, "Land Use Dynamics and Their Impact on Hydrology and Water Quality of a River Catchment: A Comprehensive Analysis and Future Scenario," *Environmental Science and Pollution Research*, vol. 32, no. 7, pp. 4124-4136, 2025. [CrossRef] [Google Scholar] [Publisher Link]

[25] Linus S. Schauer et al., "Spatial and Temporal Variability of River Water Quality," *Hydrological Processes*, vol. 39, no. 5, pp. 1-14, 2025. [CrossRef] [Google Scholar] [Publisher Link]

[26] Md. Rajaul Karim et al., "A Comprehensive Dataset of Surface Water Quality Spanning 1940-2023 for Empirical and ML Adopted Research," *Scientific Data*, vol. 12, no. 1, pp. 1-13, 2025. [CrossRef] [Google Scholar] [Publisher Link]

[27] Tymoteusz Miller et al., "Integrating Artificial Intelligence Agents with the Internet of Things for Enhanced Environmental Monitoring: Applications in Water Quality and Climate Data," *Electronics*, vol. 14, no. 4, pp. 1-44, 2025. [CrossRef] [Google Scholar] [Publisher Link]

[28] Md Galal Uddin et al., "The Role of Optimizers in Developing Data-Driven Model for Predicting Lake Water Quality Incorporating Advanced Water Quality Model," *Alexandria Engineering Journal*, vol. 122, pp. 411-435, 2025. [CrossRef] [Google Scholar] [Publisher Link]

[29] Ryan A. Blaustein et al., "Water Metagenomes Reflect Physicochemical Water Quality throughout a Model Agricultural Pond," *Frontiers in Microbiology*, vol. 16, pp. 1-11, 2025. [CrossRef] [Google Scholar] [Publisher Link]

[30] Khabat Khosravi et al., "Enhanced Water Quality Prediction Model using Advanced Hybridized Resampling Alternating Tree-Based and Deep Learning Algorithms," *Environmental Science and Pollution Research*, vol. 32, no. 11, pp. 6405-6424, 2025. [CrossRef] [Google Scholar] [Publisher Link]

[31] Abhijeet Das, "Drinking Water Resources Suitability Assessment in Brahmani River Odisha based on Pollution Index of Surface Water Utilizing Advanced Water Quality Methods," *Scientific Reports*, vol. 15, no. 1, pp. 1-19, 2025. [CrossRef] [Google Scholar] [Publisher Link]

[32] Keval H. Jodhani et al., "Sustainable Groundwater Management through Water Quality Index and Geochemical Insights in Valsad India," *Scientific Reports*, vol. 15, no. 1, pp. 1-15, 2025. [CrossRef] [Google Scholar] [Publisher Link]

[33] Zhan Xie et al., "Machine Learning Approaches to Identify Hydrochemical Processes and Predict Drinking Water Quality for Groundwater Environment in a Metropolis," *Journal of Hydrology: Regional Studies*, vol. 58, pp. 1-14, 2025. [CrossRef] [Google Scholar] [Publisher Link]

[34] Md. Abdullah Al Mamun Hridoy et al., "Advanced Machine Learning Models for Accurate Water Quality Classification and WQI Prediction: Implications for Aquatic Disease Risk Management," *Science of the Total Environment*, vol. 1008, pp. 1-21, 2025. [CrossRef] [Google Scholar] [Publisher Link]

[35] Jasha Dehm et al., "Water Quality within the Greater Suva Urban Marine Environment through Spatial Analysis of Nutrients and Water Properties," *Marine Pollution Bulletin*, vol. 213, pp. 1-18, 2025. [CrossRef] [Google Scholar] [Publisher Link]

[36] Wenwen Chenet al., "Ensemble Machine Learning for Operational Water Quality Monitoring Using Weighted Model Fusion for pH Forecasting," *Sustainability*, vol. 18, no. 3, pp. 1-20, 2026. [CrossRef] [Google Scholar] [Publisher Link]

[37] Sajad Basirian, Mohammad Najafzadeh, and Ibrahim Demir, "Water Quality Monitoring for Coastal Hypoxia: Integration of Satellite Imagery and Machine Learning Models." *Marine Pollution Bulletin*, vol. 222, 2026. [CrossRef] [Google Scholar] [Publisher Link]

[38] K. Naga Durga Saile et al., "Satellite-based Water Quality Monitoring in Telangana Region." *AIP Conference Proceedings*, vol. 3345, no. 1, 2026. [CrossRef] [Google Scholar] [Publisher Link]

Appendix

Table 10. Laboratory methods sample key WQ metric values from 25 may to 29 may 2023

DO	pH	Conductivity	TDS	Turbidity	Mean-water	Entropy-water	PSNR-water	SNR-water	Mean-moss	Entropy-moss	PSNR-moss	SNR-moss	WR	WG	WB	MR	MG	MB
11.13	8.21	248.7	125.96	8.4	171.4	5.86	22.27	18.35	100.22	6.09	21.17	15.53	22.27	171.3	217.7	50.7	139.9	199.1
11.06	9.13	248.6	125.44	10.19	169.4	6.24	22.51	19.14	100.35	6.13	21.3	15.16	22.73	167	211	46.71	113.3	180
9.9	7.68	248.2	125.08	10.68	171.1	5.54	21.66	19.4	99.77	6.04	21.44	14.35	23.76	166.7	215	43.87	85.76	177.7
9.79	7.9	248.8	125.95	11.18	169	5.78	22.25	18.57	98.75	6.3	21.14	14.84	25.36	172.1	221.7	53.05	110.3	218.3
10.37	8.77	248.4	125.86	13.4	170.4	6.34	22.16	18.11	99.51	6.03	22.75	15.6	23.04	174.3	211.1	56.5	100.9	181.7
11.32	7.95	248.2	125.15	15.19	169.3	5.97	21.35	18.2	98.83	6.08	22.11	15.74	14.64	174.8	211.4	44.57	68.54	176.9
11.94	9.25	248.9	125.98	11.54	169	5.61	21.48	18.62	99.59	6.06	22.47	16.32	22.41	172.5	215.6	57.77	58.87	185.7

12.15	**10.1**	**12.46**	**9.22**	**9.18**	**11.98**	**9.38**	**11.44**
8.11	8.59	9.26	7.67	8.9	8.63	8.22	8.46
248.5	248.5	248.9	248.8	248.9	248.6	248.8	248.9
125.79	125	125.13	125.31	125.5	125.77	125.76	125.41
10.74	11.6	13.44	14.46	8.38	12	12.53	11.08
168.6	171.2	169.6	167.9	168.1	171.3	169.6	168.9
6.24	6.03	5.58	5.55	5.48	5.75	5.74	6.15
21.93	22.07	21.92	21.64	22.71	22.23	22.84	20.96
18.38	18.07	19.46	18.97	19.01	18.63	18.66	19.44
100.14	98.41	97.71	99.95	98.58	100.12	97.72	98.8
6.23	6.54	6.13	6.26	5.97	6.46	6.01	6.29
22.01	21.99	21.53	21.08	21.95	21.08	22.01	21.3
15.81	16.32	14.6	16.25	14.73	15.95	16.28	15.37
27.33	19.49	19.34	17.6	20.7	12.38	23.12	26.21
175.5	167	177.8	175.8	174	177.6	174.2	171.3
221.5	218	220	212.1	220	210.1	221.3	219.8
52.34	57.18	45.04	55.49	54.07	44.82	44.95	59.43
129.2	99.24	68.93	44.24	94.78	99.3	55.81	134.7
205.2	239.2	184.5	195	186.5	234.3	230	182.4

Table 11. Statistical values of pixels of regions NGD WQ metrics (Sample Data)

DO	**pH**	**Conductivity**	**TDS**	**Turbidity**	**Mean-water**	**Entropy-water**	**PSNR-water**	**SNR-water**	**Mean-moss**	**Entropy-moss**	**PSNR-moss**	**SNR-moss**	**WR**	**WG**	**WB**	**MR**	**MG**	**MB**
8.93	7.5	239.33	123.59	7.09	132.52	5.95	21.87	17.67	139.3	4.49	22.35	18.4	42.14	148	240.8	52.69	42.51	163.7
8.84	7.76	228.12	115.48	5.27	134.67	6.23	22.04	18.41	139.7	4.44	23.64	19.5	41.12	148.5	239.5	52.47	42.97	163.5
9.61	7.6	228.81	118.44	7.33	136.68	6.07	20.74	17.59	139.3	4.42	23.5	18.7	42.75	154.6	237.3	58.18	39.91	166.7
8.51	7.66	232.57	121.32	7.07	131.21	6.24	22.41	18.38	140.4	5.19	24.01	18.9	39.78	152.1	243.3	52.82	39.85	168.4
9.43	7.5	226.03	116.46	6.3	131.86	5.51	22.12	17.06	137.7	6.32	22.13	19.1	43.19	145.7	244.2	53.31	40.38	169.1
9.09	7.63	239.75	117.13	5.03	135.02	6.26	22.14	18.62	140	3.65	22.3	19.5	42.41	144.3	245.5	62.9	42.43	165.7
10.19	7.5	237.95	119.02	5.14	134.11	6.19	22.39	16.75	141.4	5.33	22.98	19.6	40.17	152.3	246.4	59.42	41.53	166.9

10.03	**9.73**	**8.88**	**10.35**	**8.44**	**10.09**	**9.96**	**9.55**
7.7	8	7.57	7.95	7.57	7.69	7.61	7.67
228.41	234.19	225.2	226.16	240.38	234.84	235.68	230.74
119.44	118.75	123.45	117.46	123.81	119.91	116.46	124.65
9	6.72	8.3	7.39	9.42	8.26	7.4	5.29
137.47	133.59	138.69	136.54	139.48	135.86	132.76	133.78
5.66	6.23	5.91	6.29	5.6	5.62	6.08	5.88
21.35	22.45	21.41	21.49	21.71	22.2	22.19	22.57
16.45	17.42	18.69	18.44	17.29	17.31	16.78	17.81
137.8	141.5	140	140.3	137.8	141.3	139	138.4
6.52	6.9	5.56	6.63	6.51	6.24	5.4	5.05
22.78	24.07	23.24	22.61	22.89	23.46	22.62	23.18
18.6	18.3	19.1	18.8	18.9	18.5	19.1	19.9
36.65	43.24	43.49	41.72	39.54	42.02	44.99	41.5
152.9	154.1	152.6	149.8	149.4	151.1	144.7	155.9
249.1	244.4	245.8	237.8	249.7	245.6	240.1	252.9
55.55	48.54	62.04	49.32	59.49	51.69	52.42	56.04
42.61	39.7	40.78	40.9	40.12	40	41.49	40.77
167.1	168	170	165.7	163.8	168.7	166.3	167.5

Table 12. Statistical values of pixels of regions of pixels at different locations at the NkD Reservoir (Sample Data)

DO	**pH**	**Conductivity**	**TDS**	**Turbidity**	**Mean-water**	**Entropy-water**	**PSNR-water**	**SNR r-water**	**Mean-moss**	**Entropy-moss**	**PSNR - moss**	**SNR - moss**	**WR**	**WG**	**WB**	**MR**	**MG**	**MB**
11.13	8.21	248.7	125.96	8.4	171.4	5.86	22.27	18.35	100.22	6.09	21.17	15.53	22.27	171.3	217.7	50.7	139.9	199.1
11.06	9.13	248.6	125.44	10.19	169.4	6.24	22.51	19.14	100.35	6.13	21.3	15.16	22.73	167	211	46.71	113.3	180
9.9	7.68	248.2	125.08	10.68	171.1	5.54	21.66	19.4	99.77	6.04	21.44	14.35	23.76	166.7	215	43.87	85.76	177.7
9.79	7.9	248.8	125.95	11.18	169	5.78	22.25	18.57	98.75	6.3	21.14	14.84	25.36	172.1	221.7	53.05	110.3	218.3
10.37	8.77	248.4	125.86	13.4	170.4	6.34	22.16	18.11	99.51	6.03	22.75	15.6	23.04	174.3	211.1	56.5	100.9	181.7
11.32	7.95	248.2	125.15	15.19	169.3	5.97	21.35	18.2	98.83	6.08	22.11	15.74	14.64	174.8	211.4	44.57	68.54	176.9
11.94	9.25	248.9	125.98	11.54	169	5.61	21.48	18.62	99.59	6.06	22.47	16.32	22.41	172.5	215.6	57.77	58.87	185.7
11.44	8.46	248.9	125.41	11.08	168.9	6.15	20.96	19.44	98.8	6.29	21.3	15.37	26.21	171.3	219.8	59.43	134.7	182.4
9.38	8.22	248.8	125.76	12.53	169.6	5.74	22.84	18.66	97.72	6.01	22.01	16.28	23.12	174.2	221.3	44.95	55.81	230
11.98	8.63	248.6	125.77	12	171.3	5.75	22.23	18.63	100.12	6.46	21.08	15.95	12.38	177.6	210.1	44.82	99.3	234.3

12.15	**10.1**	**12.46**	**9.22**	**9.18**
8.11	8.59	9.26	7.67	8.9
248.5	248.5	248.9	248.8	248.9
125.79	125	125.13	125.31	125.5
10.74	11.6	13.44	14.46	8.38
168.6	171.2	169.6	167.9	168.1
6.24	6.03	5.58	5.55	5.48
21.93	22.07	21.92	21.64	22.71
18.38	18.07	19.46	18.97	19.01
100.14	98.41	97.71	99.95	98.58
6.23	6.54	6.13	6.26	5.97
22.01	21.99	21.53	21.08	21.95
15.81	16.32	14.6	16.25	14.73
27.33	19.49	19.34	17.6	20.7
175.5	167	177.8	175.8	174
221.5	218	220	212.1	220
52.34	57.18	45.04	55.49	54.07
129.2	99.24	68.93	44.24	94.78
205.2	239.2	184.5	195	186.5